

Delft University of Technology  
Master of Science Thesis in Computer & Embedded Systems Engineering

# Quality assessment of Paper Insulated Lead Covered cables using Near-Infrared Spectroscopy

Hendrikus Laurentius Maria Steman





# Quality assessment of Paper Insulated Lead Covered cables using Near-Infrared Spectroscopy

Master of Science Thesis in Computer & Embedded Systems  
Engineering

Embedded Systems Group  
Faculty of Electrical Engineering, Mathematics and Computer Science  
Delft University of Technology  
Van Mourik Broekmanweg 6, 2628 XE Delft, The Netherlands

Hendrikus Laurentius Maria Steman

30<sup>th</sup> of July 2024

**Author**

Hendrikus Laurentius Maria Steman (H.L.M.Steman@student.tudelft.nl)  
(ricksteman@live.nl)

**Title**

Quality assessment of Paper Insulated Lead Covered cables using Near-Infrared Spectroscopy

**MSc Presentation Date**

23<sup>rd</sup> of August 2024

**Graduation Committee**

Dr. Qing Wang

Delft University of Technology

Dr. Mohamad Ghaffarian Niasar

Delft University of Technology

Ir. Pjotr Muis

Duurzaam Energie Perspectief, Alliander

## Abstract

The increasing expansion of the electrical network accentuates the need for a better understanding of the quality of the existing infrastructure. Assessing the quality of the individual cables becomes instrumental in prioritizing replacements and grid reinforcements within the network. A critical evaluation of insulation quality in paper insulated lead covered cables is important to ensure a robust electricity grid. Moisture plays a key role in the degradation of the paper insulation. In this thesis a novel microcontroller based near-infrared spectroscopy system design is proposed which is able to measure the moisture content of paper insulated lead covered cable insulation with a theoretical accuracy of about  $\pm 1\%$  moisture content, while being cost effective and portable. It achieves this accuracy by making use of an outlier detection algorithm which is able to increase the accuracy of the system from  $\pm 3\%$  to  $\pm 1\%$ , by removing outliers of individual sensors and averaging the results of multiple measurements. The resulting output of the algorithm is linked to the asset number of the paper insulated lead covered cable under test, and uploaded to the cloud to enable further data analysis. The proposed near-infrared spectroscopy system performs measurements on one particular absorption band of water; the absorption band around 1450 nm. Due to the influences of stray light, a design of a paper insulation sample holder is proposed. This sample holder is customized to the used components in the design and fixes the samples in place, which limits measurement inconsistencies. A testing procedure is proposed to link the sensor output to the moisture content of the paper insulation sample. A linear relation is found between the sensor output and the moisture content of the paper insulation samples at a moisture content of 0% to 20%.



*“The ideal engineer is a composite ... He is not a scientist, he is not a mathematician, he is not a sociologist or a writer; but he may use the knowledge and techniques of any or all of these disciplines in solving engineering problems.” – N.W. Dougherty*



# Preface

During the final months of my BSc degree in Electrical Engineering, I was left with the decision whether to pursue power engineering or embedded systems in the coming years. My decision ultimately led to the latter, however power engineering always stayed an interest of mine. I was finally able to combine my two interests when the opportunity arose during the EEMCS Recruitment Days to do my thesis at Alliander. After some discussions about potential subjects, I finally landed a position at Duurzaam Energie Perspectief. One of the focuses of this subsidiary is on research and innovation. As a result, during my thesis, I was given the unique opportunity to present my work to several departments within Alliander, as well as present my findings to TenneT.

Firstly, I would like to thank my supervisors Pjotr Muis of Duurzaam Energie Perspectief, and Qing Wang. I want to give special thanks to Pjotr, who was as much invested in the project as I was. We had some good discussions about my design, and you have always been not only a tremendous help during the project but also immensely supportive, and critical when I needed it. Likewise, I would like to thank Ole Brauckmann, with whom I had good discussions related to Near-Infrared spectroscopy. Who also helped me greatly in performing the experiments and analysing the data. On top of that, I would like to thank Samir den Haan, who helped me greatly with the design and realisation of the 3D printed sample holder. In addition, I would like to thank the SOT team of Alliander: Martijn Piket, Boris Kooij and Munir Busch. Thank you for always supplying me with the necessary PILC cables when I needed them and giving me additional knowledge about the cables itself.

I would like to thank my family and friends, who were always considerate when I just kept rambling on about power cables and moisture measurements.

Finally, I would like to thank my amazing girlfriend, Valerie. During the many setbacks I faced along the way, you were always the first to pick me back up. You were always the one who made sure I kept my head high when it felt like I was lost in the chaos. I will always be grateful for your support during this final and stressful part of my academic journey.

Hendrikus Laurentius Maria Steman

Delft, The Netherlands  
30th July 2024



# Contents

<b>Preface</b>	<b>vii</b>
<b>List of Figures</b>	<b>xi</b>
<b>List of Tables</b>	<b>xiii</b>
<b>Nomenclature</b>	<b>xv</b>
<b>1 Introduction</b>	<b>1</b>
1.1 PILC cables . . . . .	1
1.2 Cable degradation . . . . .	2
1.2.1 Thermal degradation . . . . .	2
1.2.2 Electrical degradation . . . . .	3
1.2.3 Mechanical degradation . . . . .	3
1.2.4 Environmental degradation . . . . .	4
1.3 Problem Statement . . . . .	4
1.4 Thesis Outline . . . . .	5
<b>2 Literature review</b>	<b>7</b>
2.1 Depolymerisation . . . . .	7
2.1.1 Cellulose ageing . . . . .	9
2.2 Moisture effects on paper insulation . . . . .	10
2.2.1 Moisture assessment from electrical property measurements	11
2.2.2 Moisture assessment from physical property measurements	13
2.2.3 Measuring technique feasibility . . . . .	15
2.3 State of the art . . . . .	17
2.4 Project objective . . . . .	18
<b>3 System design</b>	<b>21</b>
3.1 NIR wavelength selection . . . . .	21
3.1.1 NIR sensor selection . . . . .	23
3.2 Microcontroller . . . . .	24
3.3 Hardware design . . . . .	25
3.3.1 I <sup>2</sup> C interface . . . . .	25
3.3.2 Hardware components . . . . .	26
3.4 Software design . . . . .	27
3.4.1 Measurement initialization . . . . .	28
3.4.2 NIR Sensor measurement protocol . . . . .	28
3.4.3 Mode verification . . . . .	29

3.4.4	Outlier detection algorithm . . . . .	29
<b>4</b>	<b>Experimental setup</b>	<b>33</b>
4.1	PILC paper sample holder . . . . .	33
4.1.1	Measuring distance . . . . .	35
4.2	Sensor configuration . . . . .	35
4.2.1	LED drive current and gain . . . . .	37
4.2.2	Circular buffer . . . . .	38
4.3	Testing procedure . . . . .	40
4.4	Cable information . . . . .	41
<b>5</b>	<b>Results and Discussion</b>	<b>43</b>
5.1	Resin effect . . . . .	43
5.2	Hydration curve . . . . .	44
5.3	Sensor characteristics . . . . .	46
5.4	Effects of outlier removal algorithm . . . . .	48
<b>6</b>	<b>Conclusions</b>	<b>51</b>
<b>7</b>	<b>Future Work</b>	<b>53</b>
<b>A</b>	<b>NIRS system overview</b>	<b>61</b>
<b>B</b>	<b>PCB schematic</b>	<b>62</b>
<b>C</b>	<b>Cable overview</b>	<b>63</b>

# List of Figures

1.1	Cross-section of a three-phase PILC cable, annotated with the most important layers. . . . .	2
1.2	Diagram of a partial discharge in a cavity in solid insulation. . . . .	3
2.1	Depolymerisation process of a cellulose polymer, where the long glucose chain is broken down into shorter glucose monomers. . . . .	8
2.2	Double-layer dielectric model of PILC insulation where the smaller top layer represents the oil layer present within the layers of paper insulation of PILC cables, and the larger bottom layer represents the cellulose insulation paper [26]. . . . .	11
2.3	Effects of moisture content on loss angle . . . . .	12
2.4	Shering bridge schematic and the corresponding balancing equation [15]. . . . .	13
2.5	Schematic of the principles of reflective NIRS, with a LED emitting, on the right, emitting light within the NIR range, and a photodiode on the left converting the absorbed light into a current. . . . .	14
2.6	Normal modes of water vibrations; From left to right: symmetric stretching, bending vibration, antisymmetric stretching [37]. . . . .	14
2.7	Absorption coefficients of water within the NIR range at 20°C [12]. . . . .	15
3.1	Responsivity as a function different wavelengths of photodiodes made of different materials [62]. Green is Poly(3-hexylthiophene) (P3HT), blue is Silicon (Si), red is Germanium (Ge), and black is Indium Gallium Arsenide (InGaAs). . . . .	22
3.2	The internal architecture and pins of the P13567-02CT NIR sensor [23]. . . . .	23
3.3	A block model of the system architecture, including the transferred data, where the dotted line indicates a wireless connection and the solid line indicates a physical connection. . . . .	25
3.4	The I <sup>2</sup> C protocol, annotated with the function of each bit and the transmitter of the data. . . . .	26
3.5	Annotated PCB front and back. Hereafter, the NIR sensors will be referred to by their relative positions on the PCB. . . . .	27
3.6	State machine representation of the internal functionality of the microcontroller. The order of the NIR sensors is dependent on the channels of the I <sup>2</sup> C Multiplexer, where <i>North</i> corresponds to $i = 1$ , <i>East</i> to $i = 2$ , <i>West</i> = 3, and <i>South</i> = 4. . . . .	31

4.1	The measuring setup consisting of a custom designed 3D printed sample holder, which can be screwed onto the created PCB, and a paper insulation sample between two microscope slides; Below that, the dimensions (in mm) of the 3D printed sample holder, with the lid on the left and the holder on the right. . . . .	34
4.2	Optimal sensor output with regards to distance between the sensor and the target object [23]. . . . .	35
4.3	The effects of various LED drive currents on the sensor output for dry and wet samples. . . . .	37
4.4	The settling time of the sensor output of a measurement at 8 mA LED drive current and low gain. . . . .	38
4.5	Working principle of a circular buffer, where the reader and writer can move independently. . . . .	39
5.1	Sensor output against hydration time from samples where the resin is still present. Three paper samples were used per hydration time. . . . .	44
5.2	Moisture absorption of one PILC paper insulation sample per hydration time, plotted over hydration time with the resin removed from the samples and the parameters associated with the fitted exponential saturation curve. One paper samples was used per hydration time. . . . .	45
5.3	Sensor output corresponding to two PILC paper insulation samples per hydration time with the resin removed and the parameters associated with the fitted exponential curve from (5.2). Two paper samples were used per hydration time. . . . .	46
5.4	The fitted curve of the sensor output plotted against the fitted curve of the moisture absorption of a PILC sample and the parameters associated with the fitted second degree polynomial as seen in (5.3). . . . .	48
5.5	The effect of the outlier removal algorithm on the deviation from the reference model, constructed of one moisture content measurement per hydration time. . . . .	49
A.1	Overview of the NIRS system with an insulation sample. . . . .	61
B.1	Electrical schematic of the PCB. . . . .	62
C.1	Overview of the used PILC cable with its cable tag and manufacturing year. . . . .	63

# List of Tables

2.1	Values for $E_{a,oxi}$ and $A_{oxi}$ according to studies. . . . .	10
2.2	Values for $E_{a,pyr}$ and $A_{pyr}$ according to studies. . . . .	10
2.3	Maximum absorption coefficients peaks of water at 20°C [12]. . .	15
3.1	Comparison of microcontrollers commonly used for NIRS and common alternatives, where the active energy consumption is taken as an average. . . . .	24
3.2	An overview of components used in the total NIRS system. . . .	28
4.1	The address map of the P13567-02CT, containing the settings of the sensor. . . . .	36



# Nomenclature

## Abbreviations

DP	Degree of depolymerisation
DSO	Distributing system operator
HFAC	High frequency alternating current
I <sup>2</sup> C	Inter-integrated circuit
InGaAs	Indium Gallium Arsenide
kNN	k-Nearest neighbors
LOD	Loss-on-drying
NIR	Near-Infrared
NIRS	Near-Infrared spectroscopy
PCA	Principle component analysis
PILC	Paper insulated lead covered
RCE	Resonant-cavity-enhanced
SCL	Serial clock line
SDA	Serial data line
SFCU	Scission fraction of cellulose unit
TSO	Transporting system operator
VLF	Very low frequency
XLPE	Cross-linked poly-ethylene

## Variables

$A$	Constant indicating the number of molecular collisions	[-]
$C$	Capacitance	[F]
$C_h$	Moisture saturation	[%]

$C_s$	Sensor output as paper sample reaches saturation	[ <i>Counts</i> ]
$E_a$	Activation energy	[J/mol]
$f$	Frequency	[Hz]
$I$	Current	[A]
$k$	Reaction rate	[-]
$k_h$	Moisture saturation rate	[-]
$k_s$	Sensor output saturation rate	[-]
$M_c$	Moisture content in the insulation paper	[%]
$R$	Resistance	[ $\Omega$ ]
$R_h$	Scale constant of the initial moisture content	[%]
$R_s$	Scale constant of the initial sensor output	[ <i>Counts</i> ]
$R_{gas}$	Universal gas constant	[J/(mol·K)]
$T$	Absolute temperature	[K]
$t_h$	Hydration time	[min]
$V$	Voltage	[V]

# Chapter 1

## Introduction

Electrical power cables serve as indispensable conduits within the expansive infrastructure that powers our modern world. As the global pursuit of electrification gains momentum, the integrity and reliability of these cable systems are of great interest for distributing and transporting system operators (DSO's and TSO's), who themselves are overloaded with the need for expansion and renovation, fuelled by the need for industrial electrification.

The increasing expansion of the electrical network accentuates the need for a better understanding of the quality of the existing infrastructure. Informed decisions regarding grid expansion and maintenance necessitate a comprehensive grasp of the condition of the cable. Assessing the quality of the individual cables becomes instrumental in prioritizing replacements and grid reinforcements within the network. Additionally, possibilities can be explored to increase the load on cables in good condition. Therefore, cable quality assessment needs to be done efficiently and effectively; time and cost effective for the DSO/TSO. In order to determine the quality of a power cable, one must take into account the quality of its insulation. This thesis delves into the critical evaluation of insulation quality in electrical power cables, with the focus on the older Paper Insulated Lead Covered (PILC) cables.

### 1.1 PILC cables

PILC cables are widely used in electricity grids worldwide. In Figure 1.1 a cross-section of a three-phase PILC cable is shown. PILC cable insulation is built up of layers of paper, impregnated with a mass. Therefore, PILC cables are also often referred to as mass-impregnated cables in literature. This mass exists of a mixture of oil, resin and wax [53]. Hereafter referred to as resin. In order to protect the insulation from the environment, the insulation is enclosed in a lead sheath. The PILC cable is further reinforced with galvanized steel tape and provided with an outer serving. This outer serving consists of a bitumen impregnated sheath for older cables, while newer cables are fitted with a PVC sheath.

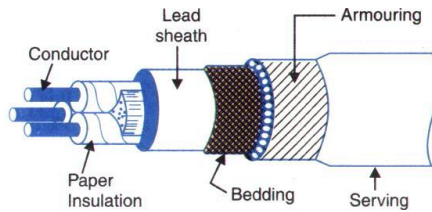


Figure 1.1: **Cross-section of a three-phase PILC cable, annotated with the most important layers.**

PILC cables used in electricity grids are often designed to last 30 to 50 years [10]. However, a lot of PILC cables within the Dutch electricity grid are much older than this. While in the past PILC was the best option, nowadays, PILC has been replaced with a more thermally robust counterpart, namely Cross-Linked Poly-Ethylene (XLPE). However, still around 47.000 kilometer of the Dutch electricity grid under the control of Alliander exists of PILC cables. The main difference between PILC and XLPE cables is the maximum temperature these cables can handle. While PILC is limited to a conductor temperature of 50°C due to the nature of the insulation, XLPE can go up to 90°C [48].

Furthermore, the way these cables are affected by moisture are widely different. XLPE is mostly affected by water-treeing, which is the process of water finding a path through the polyethylene [19]. In contrast, PILC insulation always contains a small concentration of moisture. While this is not necessarily a problem, it can accelerate degradation if moisture contents become too high [38]. PILC cables are being operated without knowing their exact condition. This can lead to unexpected failures leading to local power outages. Therefore gaining knowledge about the current condition of the paper insulation is truly valuable.

## 1.2 Cable degradation

PILC cables are subjected to high electrical stress and currents inducing an elevated temperature. Additionally, the insulation is subjected to various other kinds of stresses, all with a different nature. These stresses can cause cable deterioration in their own way and are therefore classified into the following categories: thermal, electrical, mechanical, and environmental degradation. In the following sections these stresses will be elaborated upon and their relevance to this research will be determined.

### 1.2.1 Thermal degradation

Thermal degradation is a common form of degradation. As power cables are put under load, the conductor heats up, which in turn heats up the insulation. This temperature increase is mostly due to ohmic losses within the conductor [60]. Many studies are performed to model the thermal degradation of PILC cables. All studies use the same law as a basis for their research, namely the Arrhenius law. The Arrhenius law is a formula which describes the temperature

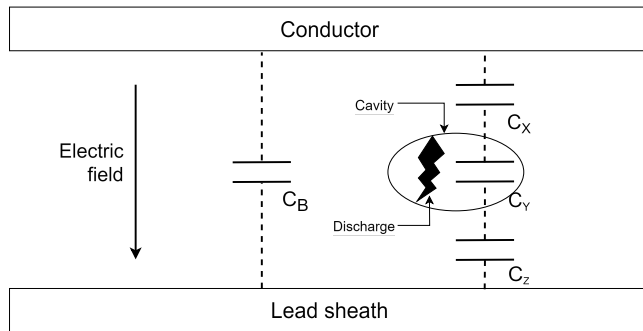


Figure 1.2: **Diagram of a partial discharge in a cavity in solid insulation.**

dependence of the reaction rate in a chemical reaction [13]:

$$k = A \cdot e^{\frac{-E_a}{R_{gas} \cdot T}}, \quad (1.1)$$

where  $A$  is a dimensionless constant indicating the number of molecular collisions resulting in the reaction,  $E_a$  is the activation energy in J/mol needed in order for the reaction to occur.  $R_{gas}$  represents the universal gas constant, which is approximately 8.314 J/(mol · K). Finally,  $T$  is the absolute temperature denoted in  $K$ . In the application of paper insulation degradation, this law describes the degradation rate of the cellulose insulation paper as a function of temperature.

### 1.2.2 Electrical degradation

Power cables under operation are naturally subjected to electrical stresses. Apart from the conductor heating up as discussed in Section 1.2.1, the continuous electrical stress can also cause deterioration due to leakage currents and partial discharges. Particularly the latter can cause accelerated degradation of the paper insulation, due to the forming of carbon in the insulation. Partial discharges occur when cavities are present within the insulation [22]. These cavities can form due to the oil within the insulation migrating caused by elevation differences, or cracks in the lead sheath. In Figure 1.2, a schematic of a partial discharge in a cavity in solid insulation is shown. The cavity disturbs the electric field within the cable and when a charge jumps the gap, a path from the conductor to the lead sheath is formed [22]. This carbonized path will cause electrical-treeing and leads to cable degradation and possibly degradation of the lead sheath. However, due to their stochastic nature, the partial discharges themselves will not be considered in this research.

### 1.2.3 Mechanical degradation

The operation of the electrical network and maintenance on established cables cause mechanical stress on the cable and its insulation. This includes, vibrations, bending, tension, and compression among other things. These mechanical stresses can cause degradation to the physical structure of the cellulose paper insulation, which reduces its insulation ability [11]. Additionally, the ground subsidence within the Netherlands causes a mechanical pull on the cables, which could lead to power failure.

However, most mechanical stresses on PILC cables are hard to quantify and several types of mechanical stress might occur simultaneously. Moreover, policies are already in place to reduce the mechanical stress on these cables. Therefore, the mechanical stress on PILC cables will not be accounted for further.

#### **1.2.4 Environmental degradation**

PILC cable insulation is covered by a lead covering sheath. This sheath will keep out any external moisture and protects the paper insulation against the environment. Overall lead is a relatively non-reactive metal and therefore particularly suitable as a protective sheath. However, lead is a soft metal, making it prone to deformation and wear. Moreover, the acids within the mass of the insulation can deteriorate the lead sheath.

Unfortunately, the outer serving of impregnated bitumen of older PILC cables often does not provide enough protection to the lead covering, leading to air and moisture getting in contact with the lead covering sheath. This moist air unfortunately leads to the degradation of the lead covering sheath, due to the corrosion taking place with oxygen and water present [25]. As a result, PILC cables often lose their lead covering sheath partially or entirely. This leads to accelerated degradation of the PILC cable. However, this process happens randomly and incidentally and thus is far from easy to model. Above all, the exposure of the insulation to the environment has no effect of its own, it simply accelerates the thermal, electrical and mechanical degradation. Therefore, lead sheath corrosion and degradation will not be regarded in further modelling.

### **1.3 Problem Statement**

As mentioned above, a critical evaluation of insulation quality in PILC cables is important to ensure a robust electricity grid and to make renovation more efficient. In order to assess the insulation, one must first compromise the outer layers of the PILC cable. Which leads to faster degradation as mentioned earlier, and therefore defeating the purpose of assessing the insulation quality in the first place. However, one exception to this exists when a new connection must be made on an existing cable within the network. In this situation the conductor must be laid bare in order to connect to the existing cable. This gives the unique opportunity to get valuable quantifiable data concerning the quality of the insulation.

What becomes apparent from Section 1.2.1 up until Section 1.2.4, is that moisture plays a key role in each category of degradation. Therefore, in order to determine the quality of the insulation paper, one must quantify the moisture content of the paper insulation. At the moment tests are performed to inspect whether or not the paper insulation contains any moisture. This test consists of dropping a sample of insulation into a tub of hot oil to see if bubbles form [34]. Not only does this not give any indication of how much moisture is present in the paper, it is also primitive, subjective and regarded as dangerous. In addition, it is often not performed by the technicians making the new connection.

Hence, this study tries to solve this issue, while simultaneously gaining valuable information about the electrical network. Additionally, if a large enough quantity of cables has been evaluated, a machine learning model could potentially be trained on the acquired data in order to extrapolate this data over the entire population of PILC cables within the network. In order to achieve this, a portable device needs to be created which reads the moisture content of a paper insulation sample. Combining this data with cable degradation models, the remaining life of the assessed PILC cable can be estimated.

## 1.4 Thesis Outline

In essence, this thesis studies the quality assessment of PILC cable insulation, with a particular focus on the quantification of the moisture content in the paper insulation. Chapter 2 formulates the theoretical basis by explaining the theories and complexities linked to moisture content in insulation material in power cables. In addition, it delves into an extensive analysis of how the moisture content is reflected into the different properties of the insulation and the available measurement techniques to assess it.

Chapter 3 constitutes a critical examination of hardware components, serving as a comparative study with evaluation criteria that encompass financial considerations, performance efficiency, and specific design requisites as well as the system design and architecture. Subsequently, Chapter 4 outlines the methodological approach of this research; the experimental setup created for the system and the systematic procedures employed in data collection.

Chapter 5 presents the findings of the measurements performed, which will describe the implications of these measurements and incorporated models to provide context to the measurements. Finally, Chapter 6 provides conclusive remarks, discussions, and Chapter 7 ends with recommendations for further research directions.



## Chapter 2

# Literature review

Moisture content plays a key role in assessing cable degradation of PILC cables, as was stated in Section 1.3. However, it is important to understand how moisture is formed within the cable insulation and which relation it has to degradation. In Section 2.1, relevant studies are explored relating the moisture content of paper insulation to degradation processes. The most prominent of which being the depolymerisation of the cellulose paper insulation. This will further link depolymerisation with the aging process of insulation paper [42]. In Section 2.2, studies will be analysed describing the effects moisture has on PILC insulation paper. This is followed up by different ways to measure these properties and thus moisture within the insulation. These methods will be analysed and challenged to the thesis objective. Finally, in Section 2.3, the state of the art will be discussed with respect to the preferred measurement technique.

### 2.1 Depolymerisation

Thermal degradation is the main driving force of insulation degradation, as stated in Section 1.2.1. It is important to note the processes which cause degradation and how one can measure this. In literature, the degree of polymerisation (DP) of the cellulose insulation is often regarded as the main indicator of deterioration [24, 30, 54]. Cellulose is a homopolymer, composed of long chains of anhydroglucose [46]. The average length of the glucose chains is regarded as the DP, and can therefore be used to describe the deterioration level of PILC cable insulation. Cellulose created from wood fibers has a DP ranging from 300 to 1100 [46]. Different aging processes can contribute to the decrease in DP. The three main processes which contribute to the aging of insulation paper are:

- **Oxidation:** degradation due to the exposure to oxygen.
- **Hydrolysis:** degradation due to the exposure to water.
- **Pyrolysis:** degradation due to the exposure to high temperatures.

These processes break down the glucose chains and reduce the average length of these chains [36]. A graphical representation of the chemical changes can be found in Figure 2.1.

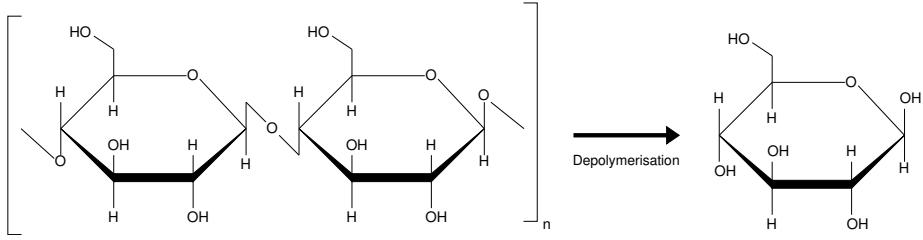


Figure 2.1: **Depolymerisation process of a cellulose polymer, where the long glucose chain is broken down into shorter glucose monomers.**

Depolymerisation is a very intricate chemical process, where much is beyond the scope of this thesis. However, what is important to note is that the byproducts produced by the depolymerisation process contain furanics,  $\text{CO}_2$ ,  $\text{CO}$ , and  $\text{H}_2\text{O}$  [24, 32]. Especially the latter byproduct is important for this thesis. By making use of the relation between the DP and the moisture content of the insulation paper, one can approximate the DP by measuring the moisture content of the PILC cable insulation paper.

In order to draw any significant conclusions from the DP of the insulation paper, a mathematical relation is needed describing the relation between DP and deterioration over time. This subject has been researched extensively in the past, and as early as 1936, Ekenstam found the equation of the Scission Fraction of Cellulose Unit (SFCU) as a function of DP [16]:

$$\ln\left(1 - \frac{1}{DP(t_0)}\right) - \ln\left(1 - \frac{1}{DP(t)}\right) = k \cdot \Delta t. \quad (2.1)$$

When  $DP(t_0)$  and  $DP(t)$  are large, and the cellulose system is homogeneous, this equation can be reduced to [45]:

$$\frac{1}{DP(t)} - \frac{1}{DP(t_0)} = k \cdot \Delta t, \quad (2.2)$$

where  $DP(t_0)$  and  $DP(t)$  denote the DP at the start,  $t_0$ , and at the end,  $t$ , of the analysed time period  $\Delta t$ , and  $k$  denotes the reaction rate constant, which is dimensionless.

By combining (1.1) with (2.2), one can describe the paper aging as a thermally activated kinetic process, often referred to as the Arrhenius relation [17]:

$$\frac{1}{DP(t)} - \frac{1}{DP(t_0)} = A \cdot e^{\frac{-E_a}{R_{gas} \cdot T}} \cdot t. \quad (2.3)$$

### 2.1.1 Cellulose ageing

Three main processes contribute to the aging of insulation paper, as described in Section 2.1. These processes occur simultaneously and are all affected by one another. Therefore, creating an accurate ageing model is a very complex task. As a result, most researchers assume the processes act independently, each in a specific temperature range. In [7], the Arrhenius relation, as seen in (2.3), has been divided in all three processes respectively for paper degradation in power transformers:

$$\frac{1}{DP(t)} - \frac{1}{DP(t_0)} = k(t) \cdot \Delta t, \quad (2.4)$$

with:

$$k(t) = \left( A_{hyd}(t) \cdot e^{\frac{-E_{a,hyd}}{R_{gas} \cdot t}} + A_{oxi}(t) \cdot e^{\frac{-E_{a,oxi}}{R_{gas} \cdot t}} + A_{pyr}(t) \cdot e^{\frac{-E_{a,pyr}}{R_{gas} \cdot t}} \right). \quad (2.5)$$

Where  $k(t)$  is the rate of degradation as a function of time and the *oxi*, *hyd* and *pyr* subscripts correspond to the oxidation, hydrolysis and pyrolysis processes respectively.

In order to draw any conclusions from this adapted Arrhenius relation, one must compute the activation energy ( $E_a$ ) and constant ( $A$ ). Extensive research has been performed on quantifying these constants. In [31], a quadratic formula has been proposed which relates the moisture content of the paper insulation with  $A_{hyd}$ :

$$A_{hyd} = 1.78 \cdot 10^8 \cdot M_c^2 + 1.1 \cdot 10^8 \cdot M_c + 5.28 \cdot 10^7, \quad (2.6)$$

where  $M_c$  is the water content in insulation paper in percentages.

The second degree polynomial function, shown in (2.6), proves that not only is moisture a byproduct of the ageing processes, but it also acts as a catalyst for accelerated ageing. Reinforcing the need for moisture measurements on existing infrastructure.

Previously, the activation energy for hydrolysis was believed to be 111 kJ/mol [17], however in [8], the author proved  $E_{a,hyd}$  to be 128 kJ/mol. Various studies have resulted in consistent findings for  $E_{a,hyd}$ .

While various studies also have resulted in consistent findings for oxidation [18, 31], as shown in Table 2.1, studies often disagree on the values for pyrolytic degradation. This can be seen in Table 2.2, where a disparity in the variables with regards to pyrolytic degradation can be seen. As a result, there is no clear consensus on what the value of  $E_{a,pyr}$  and  $A_{pyr}$  should be modelled as.

Table 2.1: Values for  $E_{a,oxi}$  and  $A_{oxi}$  according to studies.

Author	$E_{a,oxi}$	$A_{oxi}$
[18]	89	$4.6 \cdot 10^5$
[31]	89	$4.6 \cdot 10^5$

Table 2.2: Values for  $E_{a,pyr}$  and  $A_{pyr}$  according to studies.

Author	$E_{a,pyr}$	$A_{pyr}$
[9]	215.7	$4 \cdot 10^{17}$
[40]	255	$5.8 \cdot 10^{20}$
[52]	220	$7.2 \cdot 10^{20}$

Each of these processes are predominant on a different temperature range, ranging up to 140°C and above for pyrolytic degradation [6]. However, while the paper in transformers is identical to that inside of PILC cables, the temperature the paper insulation reaches in a PILC cable is much lower. Since the conductor temperature of a PILC cable is limited to 50°C [48]. Therefore the pyrolytic degradation is neglected in the proposed adapted model, since the impact of this process can not accurately be assessed. The resulting model will therefore give an optimistic indication with regards to insulation paper loss of life since the pyrolytic degradation, while minor, will be disregarded:

$$\frac{1}{DP(t)} - \frac{1}{DP(t_0)} = k(t) \cdot \Delta t, \quad (2.7)$$

with:

$$k(t) = \left( A_{oxi}(t) \cdot e^{\frac{-E_{a,oxi}}{R_{gas} \cdot t}} + A_{hyd}(t) \cdot e^{\frac{-E_{a,hyd}}{R_{gas} \cdot t}} \right). \quad (2.8)$$

Finally, this model for estimating the  $DP$  of the paper insulation can be used to estimate the expected life in years of the cable:

$$\text{Expected life [years]} = \frac{\frac{1}{DP(t)} - \frac{1}{DP(t_0)}}{k(t) \cdot 24 \cdot 365}, \quad (2.9)$$

with:

$$k(t) = \left( A_{oxi}(t) \cdot e^{\frac{-E_{a,oxi}}{R_{gas} \cdot t}} + A_{hyd}(t) \cdot e^{\frac{-E_{a,hyd}}{R_{gas} \cdot t}} \right). \quad (2.10)$$

## 2.2 Moisture effects on paper insulation

As mentioned in Section 2.1, moisture is a byproduct of degradation and accelerates degradation in insulation materials. In order to measure the moisture content in insulation paper, firstly, it is important to know which properties of insulation paper are affected by the moisture and which relation a quantifiable property of insulation paper has with respect to moisture content. The absorption of moisture in cellulose causes the molecular composition of the material to change slightly [41]. However, this change in molecular composition also has effects on the electrical properties of the material. Namely, the absorption of moisture causes the conductivity and the dielectric permittivity of the cellulose paper insulation to increase [59].

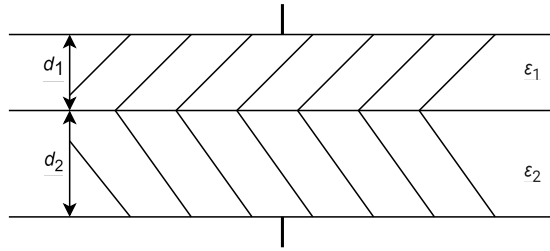


Figure 2.2: **Double-layer dielectric model of PILC insulation where the smaller top layer represents the oil layer present within the layers of paper insulation of PILC cables, and the larger bottom layer represents the cellulose insulation paper [26].**

These changes in electrical properties cause the electrical breakdown voltage of the insulation material to decrease as well. The mass-impregnated paper insulation of PILC cables can be modelled as a double layer dielectric as stated in [15]. In Figure 2.2, a graphical representation of the double layer dielectric model is shown, where the smaller top layer represents the oil layer present within the layers of paper insulation of PILC cables, and the larger bottom layer represents the cellulose insulation paper. An increase in moisture content causes the dielectric permittivity of the insulation paper to increase, denoted as  $\epsilon_2$  in Figure 2.2. This leads to a decrease in the electric field intensity in the paper insulation, which in turn causes the relative electric field strength in the oil layer to increase. This makes it easier to breakdown the insulating oil gap [26]. This will result in breakdown off the insulation material if a sufficient electrical field is applied.

### 2.2.1 Moisture assessment from electrical property measurements

Several methods exist to measure the electrical properties of insulation paper. As mentioned in Section 2.2, the electrical properties of the insulation paper are affected by the moisture content of the insulation paper. The permittivity of the insulation changes based on the moisture content of the insulation paper. This causes the capacitance of the insulation paper to change. Therefore by measuring the electrical properties of the insulation paper, one can relate the measurements to moisture content. The most prominent measuring technique to measure the electrical properties of insulation paper is the tangent delta test. This test measures the relation between the capacitive and resistive component of the insulation paper. This relation can be equated as follows:

$$\tan(\delta) = \frac{I_R}{I_C}. \quad (2.11)$$

The tangent delta test is often referred to as a Very Low Frequency (VLF) measurement, where the measuring frequencies often lie between 0.1 and 0.01 Hz. This is due to the dependence of the capacitive component on frequency. As seen in (2.12), where it becomes clear that the loss angle becomes small at high frequencies.

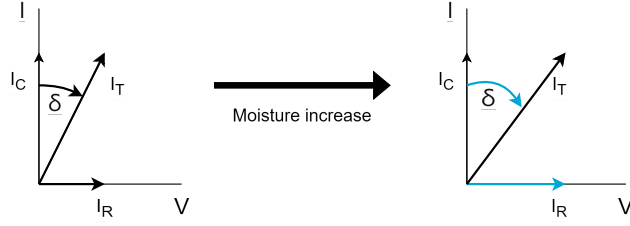


Figure 2.3: Effects of moisture content on loss angle

$$\tan(\delta) = \frac{I_R}{I_C} = \frac{\frac{V}{R}}{V \cdot 2\pi f C} = \frac{1}{2\pi f C R}. \quad (2.12)$$

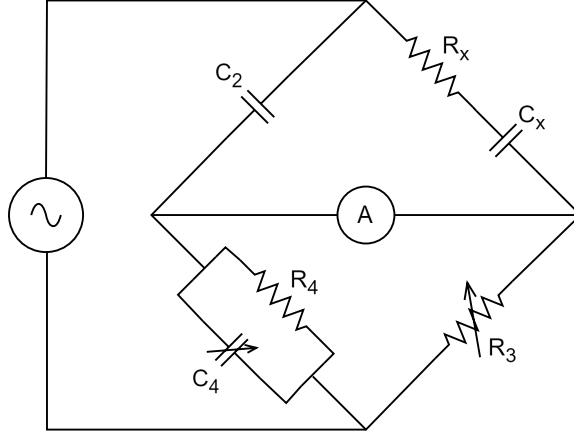
Here,  $f$  is the frequency of the supplied signal in Hz,  $C$  the capacitive component of the paper insulation in Farad, and  $R$  the resistive component of the paper insulation in Ohm.

Using this measurement method will take the entire length of the cable insulation into account, since it measures the resistive and capacitive component of the entire insulation. In order to draw conclusions from the  $\tan(\delta)$  test, measurements over a range of frequencies need to be made. Deteriorated insulation will show an increasing  $\tan(\delta)$  value over the frequency range, while ideal insulation will have a consistent  $\tan(\delta)$  value over the range [57]. Therefore, an increase in moisture content will reflect on the results of the tan delta test, and in turn give an indication of cable insulation quality. As mentioned earlier in Section 2.2, moisture causes the conductivity to increase, which in turn leads to an increased resistive current. In Figure 2.3 a representation is seen of how the loss angle increases with higher moisture content.

Similar measuring methods use the change in the capacitive component of the insulation paper. These methods are often used in agriculture. In [29], for example, where a capacitive sensor is created to measure the moisture content of the soil in order to find the ideal conditions. Here the soil is used as a dielectric. This method can also be adapted to use a sample of the paper insulation of the PILC cables as the dielectric. This is done by making use of a Shering bridge [15]. This is a common method to measure the capacitance of a sample.

In Figure 2.4, the schematic of a Shering bridge can be seen as well as its balancing conditions. Here the sample is modelled as a resistance  $R_x$  in series with a capacitance  $C_x$ . The capacitance of the sample can be measured by balancing the voltage drop across the arms of the Shering bridge using the variable capacitor  $C_4$  and variable resistor  $R_4$ . This leads to the following capacitance equation for the sample under test when separating the real and imaginary terms of the balancing equation:

$$C_x = C_2 \cdot \frac{R_4}{R_3}. \quad (2.13)$$

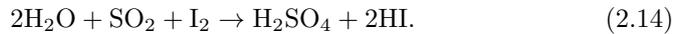


$$\left( R_x + \frac{1}{j\omega C_x} \right) \cdot \left( \frac{R_4}{1 + j\omega C_4 R_4} \right) = \frac{1}{j\omega C_2} \cdot R_3.$$

Figure 2.4: Shering bridge schematic and the corresponding balancing equation [15].

## 2.2.2 Moisture assessment from physical property measurements

All previously mentioned methods all focus on getting information from the electrical properties of the material. However, as mentioned in Section 2.2, the molecular composition of the cellulose insulation paper has also been changed due to the absorption of water. Therefore, information can also be extracted from the insulation material by exploiting the molecular changes. One of the most prominent ways in literature when extracting information from the molecular composition of a material with regards to water content, is using Karl-Fischer titration [44]. This method makes use of the well-known Bunsen reaction:



By making use of this reaction and the ensuing mole ratio, the molecular weight of absorbed water in a material can be extracted. This can be compared to the weight of the sample, resulting in a relative moisture content. Similarly, a method often used in literature is a method of heating the material in an oven in an attempt to extract all the absorbed water by evaporating it, often referred to as the Loss-on-drying (LOD) method [44]. Again by comparing this to the original weight of the sample, the relative moisture content of the sample can be determined.

Lastly, due to the absorption of water in the cellulose insulation material, the material reacts differently to electromagnetic radiation. This includes visible light, as well as infrared radiation. Therefore, a method often used in agriculture can be used. This method is called Near-Infrared spectroscopy (NIRS) [55].

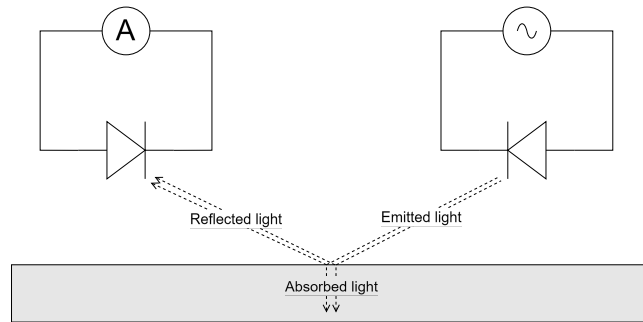


Figure 2.5: Schematic of the principles of reflective NIRS, with a LED emitting, on the right, emitting light within the NIR range, and a photodiode on the left converting the absorbed light into a current.

This method involves the monitoring of the reflectance of light within from a material. The Near-Infrared (NIR) wavelengths can range from roughly 750 nm to 2500 nm. In Figure 2.5, the principle of NIR spectroscopy is shown.

In Figure 2.5, you can see that a photodiode will generate a current based on the intensity of the reflected light from the sample. The intensity of the reflected light is closely related to the absorbance of the material for a specific wavelength. This is due to a phenomenon called molecular vibration. Molecular vibration causes the nuclei in a molecule to vibrate around their equilibrium position [4]. For water molecules, these molecular vibrations are shown in Figure 2.6, where H-O-H symmetric stretching, bending, and antisymmetric stretching vibrations are shown. In spectroscopy, photons are absorbed by the material and this induces vibrational transitions [4].

In order to find the concentration of moisture in insulation paper, the right wavelength has to be chosen such that the absorbance of light is mostly related to moisture content. In [12], the absorption spectrum of liquid water at 20°C has been investigated in the NIR spectrum. The authors found that water has five prominent absorption bands at the wavelengths of: 0.76, 0.97, 1.19, 1.45 and 1.94  $\mu\text{m}$ . This can be seen in Figure 2.7, where the absorption coefficients are plotted against the wavelengths in the NIR spectrum. From Table 2.3, it becomes apparent that especially the wavelengths of 1.45 and 1.94  $\mu\text{m}$  show promising absorption coefficients for the detection of moisture in a solid material.

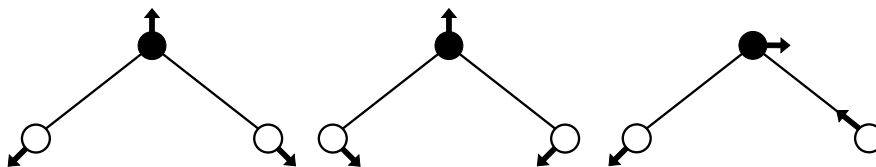


Figure 2.6: Normal modes of water vibrations; From left to right: symmetric stretching, bending vibration, antisymmetric stretching [37].

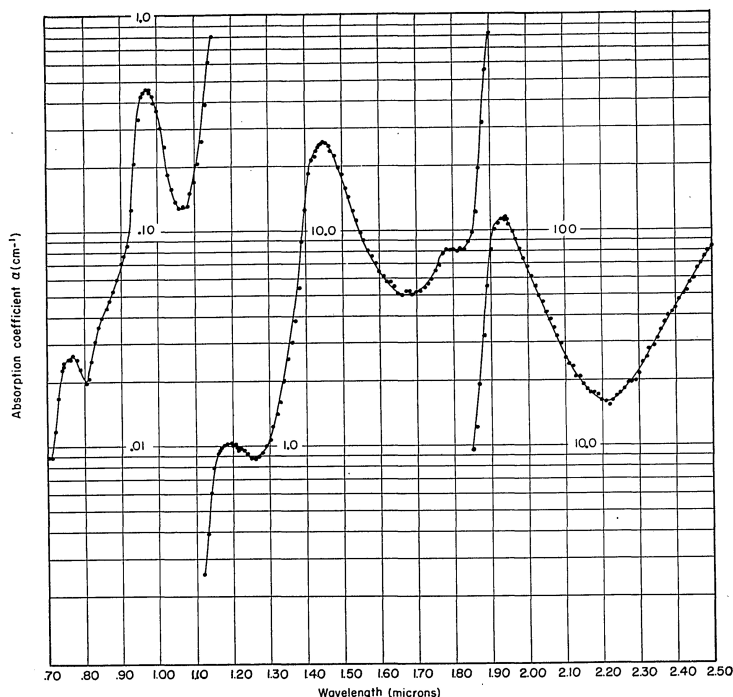


Figure 2.7: Absorption coefficients of water within the NIR range at 20°C [12].

Table 2.3: Maximum absorption coefficients peaks of water at 20°C [12].

Wavelength ( $\mu\text{m}$ )	Wavelength of max. absorption ( $\mu\text{m}$ )	Absorption coefficient at max. absorption ( $\text{cm}^{-1}$ )
0.70 - 0.90	0.76	0.026
0.90 - 1.15	0.97	0.46
1.15 - 1.35	1.19	1.05
1.35 - 1.80	1.45	26.0
1.80 - 2.50	1.94	114.0

### 2.2.3 Measuring technique feasibility

After having discussed the different ways in which moisture content can be assessed in PILC cable insulation, it is important to compare the feasibility of these methods with respect to the system requirements. As stated previously in Section 1.3, the device needs to be portable, hence most system requirements are related to the need for a portable device and the constraints which are associated with that.

The tangent delta test is a great way to determine the quality of insulation paper, however the measurement is affected by the entire cable and all its connections. Transmission systems are almost never homogeneous and each com-

ponent has an influence on the outcome of the tangent delta test. Transmission systems often consists of different types of cables with different ages and often different insulation types. Not only this, but the joints on the cable also impact the measurement. In [39], a High Frequency Alternating Current (HFAC) tangent delta measurement method is proposed to identify the effects of joints on the tangent delta measurement. However, this method requires large and expensive equipment, and therefore is not viable in a system which needs to be portable.

A traditional tangent delta measurement will not give any reliable information about PILC cables under test while it is still part of the network. Only by extracting a large part of cable from the network can this technique be used to determine the properties of the PILC cable. In [61], an attempt has been made to design a system which can perform tangent delta measurements online by injecting a VLF signal. However, it also mentions that at present the design is not accurate enough to replace the traditional tangent delta measurement. As a result, the tangent delta test is not viable for the desired online and portable solution.

The same holds for the breakdown voltage test. Since this test can only be performed offline, while destroying the insulation in the testing process. Other measurement methods, such as Karl-Fischer titration and the LOD method, are also deemed not viable due to their offline nature. However, these methods could potentially be used as a reference method for other online measurement methods which lack the capability to relay quantifiable data on its own.

Both the Shering bridge method and NIRS are fitting solutions for an online measurement. However, they are both not without their drawbacks, since both these methods are reliant on a reliable reference method in order to draw conclusions out of the measurement. Often used reference methods are either Karl-Fischer titration or LOD [44]. The quantitative data of the reference method is then used to create a calibration model for the online measuring instrument. This model will predict the moisture content of a sample based on the output of the online measuring instrument.

To sum up, most methods lack the capability to be used in an online portable measurement. This hard constraint therefore renders most methods unfeasible. In addition, most innovations on these offline measurement methods still lack the reliability when these methods are adapted to an online measurement. As a result, the Shering bridge and NIRS method seem the most viable options. The Shering bridge relies on a custom and accurate capacitive sensor. However, a capacitive sensor is dependent on many factors, such as constant pressure, temperature and placement of the sample. Furthermore, the order of magnitude of the capacitive sensor output is fairly small, making it sensitive to errors. As a result, NIRS is deemed to be the best possible solution.

## 2.3 State of the art

After having determined the best option for the moisture assessment of the cellulose insulation paper in Section 2.2.3, it is important to note what the current state of knowledge and innovation is in the field of NIRS. In addition, it is important to note how this project can contribute to the already existing literature.

Due to the more readily and commercially available hardware components, NIRS has gained a lot of attention in literature in recent years. NIRS systems are already popular measurement techniques in several fields. Studies regarding the technique of non-destructive analysis date as far back as the year 1977 [58]. In agriculture, NIRS is often used to determine soil quality or ripeness of fruits and vegetables. For instance, in [20], a device is designed to non-destructively predict the firmness and acidity of a mandarin. They make use of a very broad spectral range of 400-2350 nm in order to draw multiple conclusions from the resulting reflectance spectra. Similar studies have also been performed on different kinds of fruits. For example, in [49], citrus oils have been analysed using NIRS. Here a comparably broad spectral range of 1100-2500 nm is used, with the most interest in the absorption bands of C-H stretching at 1634-1766 and 2250-2350 nm. In addition, this study performs Principle Component Analysis (PCA) to identify the most valuable components in the broad reflectance spectrum.

In [49] is mentioned that the specific absorption band of C-H stretching are of particular interest. This means that a very broad reflectance spectrum is unneeded in order to draw conclusions. This statement is further supported by [5]. In this study the soluble solids content in fruits is evaluated using NIRS. This study uses carefully selected wavelengths within the entire spectral range in order to reduce the amount of data points. A predictive model is constructed using these selected data points, and this did not worsen the predictive accuracy as compared to using all the data points. Additionally, in [50] they mention a high correlation between absorbance at 676 nm and sugar content in different types of melons.

All previous mentioned studies were conducted using large equipment. However, in [21] the researchers stress the importance of an integrated near-infrared spectral sensor for more cost effective and less complex solutions for industrial and consumer applications. The NIR spectral sensor is created by introducing a small array of resonant-cavity-enhanced (RCE) photodetectors, each with a distinct spectral response operating in the 850–1700 nm wavelength range. This study shows that by using a photodetector fitted for a specific range, reflective spectroscopy can be performed. This effectively changes the need for large equipment, and opens the way for tailor-made specific solutions.

Additionally, microcontroller based systems are becoming more prominent in recent studies. In [14], an Arduino Uno is used in combination with an AMS AS7263 spectrometer sensor. The authors propose a system in which the integrated NIR 6-channel sensor in the AS7263 measures the intensity of the reflected light. This data is then communicated to the Arduino by making use of an Inter-Integrated Circuit (I<sup>2</sup>C) connection. The data is then processed to generate a

regression model with which the sample can be classified by making use of a k-Nearest Neighbors (kNN) algorithm.

Lately, with the rise in microcontroller based NIRS systems, NIRS gains a lot of interest in the medical field as well. NIRS makes it possible to, for example, perform measurements on bodily fluids without having to puncture the skin due to the high capability of penetrating deep into skin [33]. For example, several studies were performed with regards to non-invasively measuring the glucose level of blood [28, 47, 27]. In [47], a system is proposed, again, making use of an Arduino UNO. This is combined with a NIRS system consisting of a 940 nm LED and a compatible photodiode. The 940 nm LED is carefully chosen due to complications associated with the non-invasive analysis. Namely, human blood consists, for a large percentage, of water. The water molecules present in the blood will partly absorb the emitted light. As seen in Figure 2.7, the chosen wavelength will minimize this effect while keeping the penetrative benefits. The resulting electrical current generated by the photodiode is then converted using the analog to digital converter (ADC) within the Arduino UNO.

Finally, in [27], a glucose measuring system is proposed which combines a NIR LED and a photodiode with a Raspberry Pi. The authors claim that 97% of the measurements made by their microcontroller based NIRS system fall within the acceptable range set by the industry standard ISO 15197:2013, which specifies requirements for glucose monitoring systems. They further claim that there is no significant difference between commercially available glucose meters and their non-invasive microcontroller based NIRS system.

## 2.4 Project objective

In this literature review the effect of moisture on PILC cable insulation has been thoroughly discussed. Additionally, existing models relating moisture content, and other effects, in PILC cable insulation to degradation have been explored. Furthermore, a qualitative study has been done comparing different methods of moisture assessment both by measuring electrical properties and physical properties. From this it became clear that NIRS is deemed as the best solution. Finally, the current state of the art has been analysed in order to define the baseline and set the goals for this thesis.

The main objective of this thesis is to create a portable device capable of measuring moisture content in PILC cable insulation. This will be done by creating a microcontroller based NIRS system. A model will be calibrated by making use the LOD industry standard method for determining moisture content. This model will be used to convert the measurements of the online measuring instrument to useful quantitative data of the moisture content.

Secondly, an uniform measuring environment must be created in order to have reliable measurements at different locations and environmental light intensities. By having an uniform measuring environment, measurements are no longer subject to fluctuations from outside factors, thus creating a reliable sensor.

Lastly, a model must be created in order to link the sensor output to a more useful indicator; moisture content of the paper insulation sample. Additionally, it is important to link the resulting data from the measurements to cable asset numbers, which each cable in the Dutch electricity grid already has. This data can then be packaged, enabling a deeper understanding of the PILC assets within the network.



## Chapter 3

# System design

The main objective of this thesis is to create a portable device capable of measuring moisture content in PILC cable insulation, as discussed in Section 2.4. From the critical evaluation in Section 2.2.3, a microcontroller based NIRS system proved to be the most viable option. The proposed NIRS hardware must be portable above all. Therefore, the requirements related to the NIRS hardware are further analysed in this chapter. While an external power supply will not be discussed, the energy consumption of the system will be taken into account. The following sections aim to provide a clear overview of the technical foundation of the system. Additionally, the design decisions and system architecture are discussed, along with the challenges encountered and the implemented solutions.

### 3.1 NIR wavelength selection

The most fundamental component of the system design is the NIR sensor. The ability of the system to accurately capture in order to analyze the specific wavelengths of interest are dependent on the performance of the NIR sensor. As a result, careful consideration must be given to the wavelengths of the LED and photodiode to ensure optimal sensitivity in detecting the desired features of the PILC cable paper insulation sample.

Studies have shown that a full spectrum analysis is unnecessary, since specific absorption bands are only featured at certain wavelengths, depending on the molecule of interest. For example, in [5] and [49], only a partial spectrum, or only a few distinct wavelengths, are used to build the models upon. Proving that models can be created without a full spectrum analysis. In the NIR spectrum, moisture shows a high absorption coefficient for the wavelengths of 1.45 and 1.94  $\mu\text{m}$ , as mentioned in Section 2.2.2. As a result the NIR spectrum of the sensor should be concentrated around one of these wavelengths.

When a single wavelength is used, it is crucial to determine whether the absorption band related to moisture is isolated at that wavelength. In other words, no other absorption band should overlap the moisture related absorption band at this wavelength. If another absorption band does overlap, the sensor might detect differences in molecular composition unrelated to moisture content.

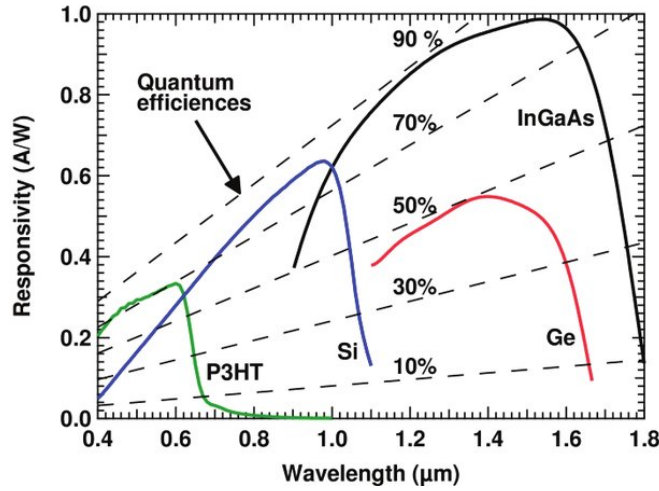


Figure 3.1: Responsivity as a function different wavelengths of photodiodes made of different materials [62]. Green is Poly(3-hexylthiophene) (P3HT), blue is Silicon (Si), red is Germanium (Ge), and black is Indium Gallium Arsenide (InGaAs).

The wavelength of  $1.94 \mu\text{m}$  shows the most promising absorption coefficient for the detection of moisture in a solid material. However, commercially available photodiodes with a peak responsivity at a wavelength of around  $1.94 \mu\text{m}$  are often very expensive, due to the need for a more sophisticated material in comparison to silicon. The responsivity of a silicon photodiode heavily drops at wavelengths above  $1 \mu\text{m}$ , as shown in Figure 3.1. As a result, photodiodes with a peak wavelength of around  $1.94 \mu\text{m}$  are deemed unsuitable for this application.

In contrast, Indium Gallium Arsenide (InGaAs) photodiodes typically have a significant decline in responsivity at wavelengths above  $1.6 \mu\text{m}$ , as shown in Figure 3.1. Therefore, an InGaAs photodiode with a peak responsivity at a wavelength of around  $1.45 \mu\text{m}$  is a practical choice. While photodiodes of this material are more expensive in comparison to silicon based photodiodes, the gain in responsivity, as mentioned in Section 2.2.2, is significant. Consequently, a minor change in moisture content can be more accurately detected. Furthermore, the isolation of the moisture absorption band at  $1.45 \mu\text{m}$  is fairly strong. Research shows that specifically sugars show no absorption at this wavelength [56]. This is a beneficial characteristic of this absorption band, since PILC insulation is made of cellulose. As mentioned in Section 2.1, cellulose is a homopolymer composed of long chains of glucose. As a result, the  $1.45 \mu\text{m}$  absorption band of moisture is sufficiently isolated. Therefore, an InGaAs photodiode with a peak responsivity at a wavelength of around  $1.45 \mu\text{m}$  is chosen in this design.

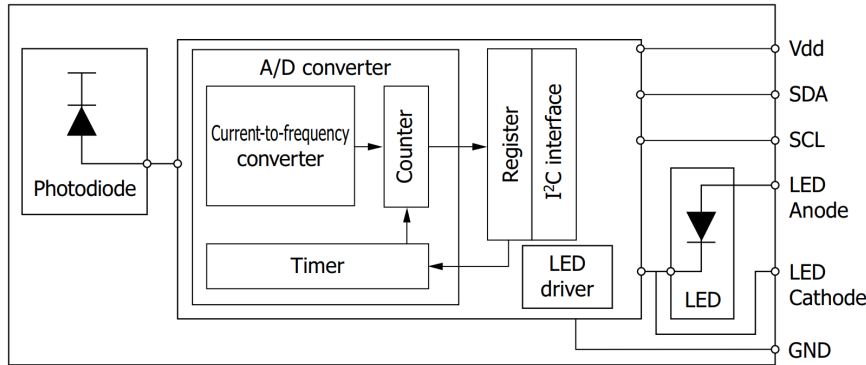


Figure 3.2: The internal architecture and pins of the P13567-02CT NIR sensor [23].

### 3.1.1 NIR sensor selection

Based on the analysis of Section 3.1, the P13567-02CT InGaAs NIR sensor by Hamamatsu was selected as a fitting component for the design of the NIRS system. As previously mentioned in Section 3.1, an InGaAs NIR sensor is relatively expensive. The cost of the P13567-02CT InGaAs NIR sensor ranges from €16 to €32 per sensor, based on the order quantity.

The internal architecture of the P13567-02CT NIR sensor is shown in Figure 3.2. This NIR sensor has been specifically selected due to the internal ADC in the chip. This enables the sensor to communicate the sensor output digitally over an I<sup>2</sup>C to the microcontroller. The sensor output is saved as an integer value, hereafter named *Counts*, in the output register. The digital communication through I<sup>2</sup>C ensures a stable and reliable data transmission, in contrast to analog signals which is susceptible to noise. Additionally, it eliminates the need for additional components necessary for handling analog signals.

The photodiode and LED present in the P13567-02CT NIR sensor are also optimized for each other. This ensures that the components work seamlessly together, and enhances the consistency of the measurements in comparison to an analog counterpart. All in all, the benefits of the packaged system, which is provided by the P13567-02CT, outweigh the cost.

However, while it is previously mentioned in Section 3.1 that a single wavelength measurement is able to sense a change in moisture content if the wavelength is sufficiently isolated, it does not come without its drawbacks. Namely, anomalies caused by external influences, such as stray light, will be much harder to detect in a single wavelength system as opposed to a system which measures on a wider spectrum. Consequently, this has to be taken into account in the system design, such that external influences will be reduced as much as possible.

Table 3.1: Comparison of microcontrollers commonly used for NIRS and common alternatives, where the active energy consumption is taken as an average.

Microcontroller	Processor	Clock Speed	Memory	Connectivity	Cost	Active Energy Consumption
Arduino Uno R4 WiFi	ARM Cortex-M4	48 MHz	32 KB SRAM, 256 KB Flash	UART, I <sup>2</sup> C, Wi-Fi	€30	≈ 70 mA [3]
Arduino Due	ARM Cortex-M3	84 MHz	96 KB SRAM, 512 KB Flash	UART, I <sup>2</sup> C	€40	≈ 80 mA [1]
Raspberry Pi Pico	ARM Cortex-M0+	133 MHz	264 KB SRAM, 2 MB Flash	UART, I <sup>2</sup> C	€5	≈ 30 mA [35]
Expressif ESP32	Tensilica Xtensa LX6	240 MHz	520 KB SRAM, 16 MB Flash	Bluetooth, Wi-Fi, I <sup>2</sup> C	€10	≈ 160 mA [51]
Arduino Nano 33 IoT	ARM Cortex-M0+	48 MHz	32 KB SRAM, 256 KB Flash	Bluetooth, Wi-Fi, I <sup>2</sup> C	€20	≈ 30 mA [2]

## 3.2 Microcontroller

A fitting microcontroller has to be selected for a NIRS system with a focus on low power consumption and data storage on the cloud. Additionally, the designed NIRS system has a relative low computational intensity in combination with a standby time of the NIR sensor of at least 400 ms [23]. This makes that a microcontroller with a high processing power only has marginal benefits.

Microcontroller based NIRS systems have gained increased attention in recent research, as discussed in Section 2.3. Many studies have used the same microcontrollers for these applications, namely the Arduino UNO and Raspberry PI. However, the latter is considered as too powerful for the scope of this design. Consequently, the Raspberry Pi Pico is further considered, since it is more in line with the hardware demands of this design. Table 3.1 provides an overview of the most common microcontrollers used for NIRS and common alternatives for the microcontrollers used in literature.

When evaluating the microcontrollers from Table 3.1, it becomes apparent that the Arduino Due is too costly when comparing its specifications to the alternatives. Additionally, it will not provide any additional benefits over the other mentioned microcontrollers. Furthermore, the Raspberry Pi Pico will require additional modules in order to have WiFi connectivity. This not only will increase the relative cost of this microcontroller, but also increases the power consumption and complicates the architecture. The Arduino Uno R4 WiFi is a compelling choice for this application. However, in comparison to the Arduino Nano 33 IoT it does not provide enough benefits to compensate for the increased cost, area and energy consumption. Finally, the Expressif ESP32 stands out for its high processing power at very low cost. However, since the designed NIRS system has an overall relative low computational intensity, the increased processing power does not outweigh the cost of the higher energy consumption.

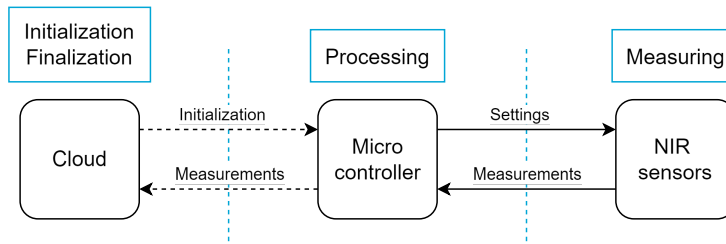


Figure 3.3: **A black model of the system architecture, including the transferred data, where the dotted line indicates a wireless connection and the solid line indicates a physical connection.**

In summary, for a NIRS system with a focus on low power consumption and data storage on the cloud, the Arduino Nano 33 IoT and ESP32 stand out as the most balanced choices. The Arduino Nano 33 IoT offers lower power consumption and ease of use with built-in connectivity, while the ESP32 provides larger memory and higher processing power, at the cost of higher active power consumption. As a result, the Arduino Nano 33 IoT is considered the best suitable microcontroller for this design.

### 3.3 Hardware design

In Figure 3.3, a black box model of the NIRS system can be seen. An overview of the system can be found in Appendix A. The microcontroller will be initialized over a Wi-Fi connection. The necessary data, which contains the measuring mode, will be send by the user from the cloud. The different measuring modes will be discussed in Section 3.4. Hereafter, the microcontroller will initialize the P13567-02CT NIR sensors using the settings discussed in Section 4.2. In order to average out measurement fluctuations in the final result, the NIRS system utilizes four NIR sensors. The measurements made by these four NIR sensor will be processed by the microcontroller. The microcontroller terminates the measurement cycle after the measurements have stabilized, which will be discussed in Section 4.2.2. Subsequently, depending on the measuring mode, the microcontroller will run the measurement through an algorithm, as discussed in Section 3.4.4. Finally, by making use of the on-chip Wi-Fi module, the final results will be send back to the cloud.

#### 3.3.1 I<sup>2</sup>C interface

The P13567-02CT NIR sensors are connected to the microcontroller by making use of an I<sup>2</sup>C interface. In I<sup>2</sup>C, two bi-directional lines are needed: Serial data line (SDA) and Serial clock line (SCL). As the name suggests, the SDA carries the data and SCL carries the clock signal to ensure synchronized data transfer. Both lines are default high to indicate that no data is being communicated. The internal pull-up resistors of the microcontroller can be used to pull the lines high.

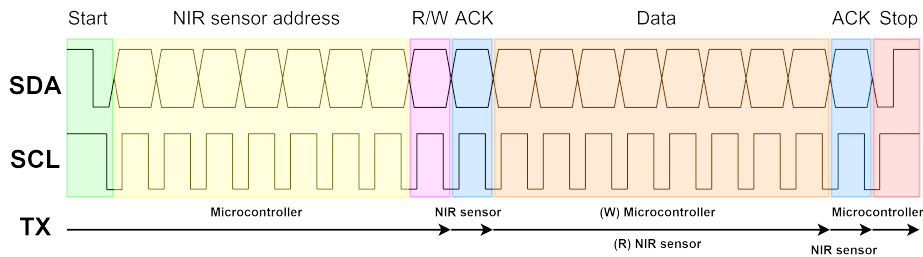


Figure 3.4: **The I<sup>2</sup>C protocol, annotated with the function of each bit and the transmitter of the data.**

In Figure 3.4 the I<sup>2</sup>C protocol is shown annotated with the function of each bit. The data is transferred in bytes. After each byte the receiver indicates that the data is received. This enables the microcontroller to detect potential errors in the I<sup>2</sup>C protocol when it does not receive an acknowledgement after sending a byte. The I<sup>2</sup>C protocol is relatively slow with the high speed mode having a frequency of 400 kHz. However, this imposes no limitations on the entire system, due to the fact that the NIR sensors are much slower, due to their standby time of at least 400 ms.

### I<sup>2</sup>C multiplexer

I<sup>2</sup>C makes use of 7-bit addressing. This allows the microcontroller to have communication between multiple sensors. Communication can be started between each device attached to the the SDA and SCL lines. However, the P13567-02CT sensors have a fixed address of 0x2A. I<sup>2</sup>C makes it impossible to have communication with multiple devices which have the same address. As a result, the design of the system has been adapted to include the I<sup>2</sup>C multiplexer PCA9548A. The PCA9548A I<sup>2</sup>C mux contains eight channels, which can be selected by calling the address of the PCA9548A and writing the channel number to its internal register. This opens the channel and allows communication with one NIR sensor at the time.

### 3.3.2 Hardware components

Due to the P13567-02CT NIR sensor having an unusual custom packaging, a custom PCB was necessary in order to fit the NIR sensors. An overview of the final designed PCB can be seen in Figure 3.5. The schematic of the PCB can be found in Appendix B. As mentioned in Section 3.3.1, an I<sup>2</sup>C multiplexer was needed in order to communicate with multiple NIR sensors. The need for a custom designed PCB allowed for the design to be adapted to the chosen PCA9548A I<sup>2</sup>C multiplexer. As a result, the dimensions of the PCB are adapted to the pins on the PCA9548A. This eliminates the need for additional wiring, which reduces the chance for reliability issues in the I<sup>2</sup>C communication protocol. Additionally, the dimensions of the PCB are adapted to ensure a reliable measurements. This is further explained in Section 4.1.

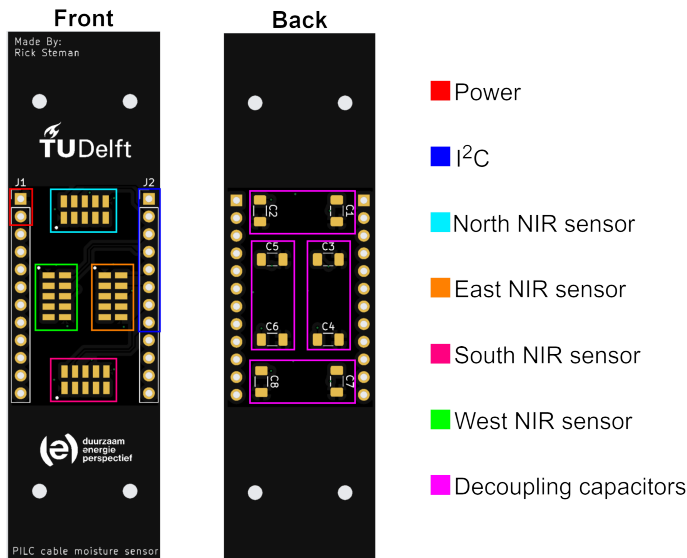


Figure 3.5: Annotated PCB front and back. Hereafter, the NIR sensors will be referred to by their relative positions on the PCB.

In order to reduce the change of light reflections and scattering, the PCB itself is manufactured in black. Furthermore, the decoupling capacitors, with a capacitance of  $66 \mu\text{F}$  and  $0.1 \mu\text{F}$ , as seen in Appendix B, are mounted at the backside of the PCB in order to further reduce any potential scattering. Due to the  $3.3 \text{ V}$  supply voltage of the NIR sensors, the DC bias characteristics of the decoupling capacitors has to be taken into account in order to ensure their expected functionality. An overview of all components used in the design of the NIRS system are listed in Table 3.2.

Unfortunately, due to the fragility of the P13567-02CT NIR sensor, two sensors were damaged during assembly. The *East* NIR sensor is sadly heavily damaged, resulting in the NIR sensor not responding to I<sup>2</sup>C commands, rendering it unusable. Additionally, the *North* NIR sensor is slightly damaged on the top epoxy layer right above the photodiode of the sensor. This leads to the photodiode not optimally absorbing the reflected light, causing the measurements from the *North* NIR sensor to be not as reliable in comparison to the *South* and *West* NIR sensors, which will be discussed in Section 5.3. However, due to the relative high cost and long shipping time of the NIR sensors, the broken sensors are not replaced in this design.

### 3.4 Software design

The internal software design of a system could often be difficult to understand. By making use of a state machine representation the behaviour of the software design is simplified. State machines clearly define how the system responds to various events. In this chapter, the software design of the NIRS system will be discussed based on the state machine representation shown in Figure 3.6.

Table 3.2: An overview of components used in the total NIRS system.

Component	Function	Quantity	Price	Total
Arduino Nano 33 IoT	Microcontroller	1	€20.00	€20.00
P13567-02CT	NIR sensor	4	€16.00	€64.00
PCA9548A	I <sup>2</sup> C Multiplexer	1	€2.00	€2.00
Capacitors	Decoupling	8	€0.30	€2.40
<b>Total</b>				€88.40

### 3.4.1 Measurement initialization

Firstly, the system requires an asynchronous input from the user in order to start. This input is provided by the user over a Wi-Fi connection. The command send will contain either an indication that the system must be used in test mode or measuring mode. The difference in these modes lies in the output of the system. Test mode will initialize the system to output the raw data collected by the NIR sensors, which enables the user to analyze the data manually. The raw data acquired in this mode can be used for future development or to calibrate the NIRS system.

Instead of indicating that the system must be used in test mode, measuring mode will require the user to specify the asset number of the cable under test. This mode is predominantly intended for moisture measurements of cables in operation. Therefore it is important that the moisture content is linked to an asset number, and this ensures that the measured moisture content is linked to the asset number when the data is send to the cloud. In contrast to test mode, where the raw data is send to the cloud, in measure mode the raw data will be converted to an equivalent moisture content. The difference in data processing between the two modes will be further discussed in Section 3.4.3.

### 3.4.2 NIR Sensor measurement protocol

After the system has initialized the test flag to be off or on, the NIR sensors start their measurement protocol. The measurement protocol itself is not affected by the way the system is initialized. The settings of the NIR sensors are fixed and can not be changed by the user without changing the software design. The settings used by the NIR sensors in this protocol will be further discussed in Section 4.2.

Each paper insulation sample will obviously react differently to the emitted light of the LED based on the moisture content of the sample. As a result, the system is designed to take repetitive short measurements of each sample, instead of longer measurements. This procedure ensures that the microcontroller has the control of when the measurement protocol should be terminated. By designing the system this way, the microcontroller is able to analyse the raw data of each short measurement and can terminate the measurement at the right time. The termination of the measurement protocol is more thoroughly explained in Section 4.2.2.

After the raw output data of the NIR sensor has reached a steady-state, the NIR sensor is turned off. Subsequently, the following NIR sensor will be subjected to the same measuring protocol. This process will continue until the last NIR sensor has saved its steady-state output in the output array (*Output*). The system is designed such that it measures two paper insulation samples of the same PILC cable during one entire cycle. This way, the reliability of the results are increased when the system is initialized in measure mode. The system waits on a second Wi-Fi packet send by the user to indicate that the second sample is correctly placed. Thereupon, the measurement protocol will repeat and the output array will be appended by the raw NIR sensor output of the second sample.

### 3.4.3 Mode verification

Following the termination of the measuring protocol, the initialization flag is used to determine how to process the raw output data (*Output*) of the NIR sensor. In case of the system being initialized in measure mode, the raw data in *Counts* of the NIR sensors, which are saved in the output array, will be converted to an equivalent moisture content. This is denoted as  $F(\textit{Output})$  in Figure 3.6. This moisture content is based on the moisture estimation model discussed in Section 5.3.

In contrast, if the system is initialized in test mode, the raw output data of the NIR sensors will be left untouched. This ensures that the user can interpret this data without interference from a model. This provides the user with the unbiased data in *Counts*, which can be used to further refine the existing models or aid in any other future developments.

### 3.4.4 Outlier detection algorithm

Finally, if the system is initialized in measure mode, the output array will be checked for outliers in order to increase the accuracy of the design. The outliers will be removed by the outlier removal algorithm as provided in Algorithm 1. For this design the outlier detection algorithm is mainly reliant on the *West* and *South* sensors. As mentioned in Section 3.3.2, the *East* sensor is unusable, and the *North* sensor provides less reliable results. As a result, only the average of the two measurements from the *North* sensor will be used to detect the outliers.

The proposed algorithm for the current NIRS system starts by checking the deviation between the measurements made by the *West* and *South* sensors. When these measurements are within an acceptable deviation of 5% moisture content between both NIR-sensors, the average of these moisture measurements is being output as the result.

If these individual measurements are not within that range, first the average of the measurements of the *West* and *South* sensors are computed and rated against a deviation of 5% moisture content between the averages of the sensors. This is done because testing proved that local differences within a sample can cause individual measurements of the same sensor to deviate a lot, however this is averaged out when taking multiple measurements into account.

---

**Algorithm 1** Outlier Removal Algorithm

---

```
1: Output array; moisture content equivalent of sensor West and South:
2:  $O[West_1, West_2, South_1, South_2]$ 
3:
4: if  $\overline{\max(Output) - \min(Output)} \leq 5$  then
5:    $Result = \overline{Output}$ 
6: else
7:   Compute average of measurements, sensor West and South;  $Avg_W, Avg_S$ 
8:   if  $-5 \leq Avg_W - Avg_S \leq 5$  then
9:      $Result = \overline{Output}$ 
10:  else
11:    Compute average of remaining sensor, North:  $Avg_N$ 
12:    Append  $Output$  array with  $Avg_n$ 
13:    Sort  $Output$  array;  $O[West_1, West_2, South_1, South_2, Avg_N]$ 
14:    Pop first and last element of  $Output$  array;  $O[1, 2, 3]$ 
15:    if  $\overline{\max(Output) - \min(Output)} \leq 5$  then
16:       $Result = \overline{Output}$ 
17:    else
18:       $Result = "No result"$ 
19:    end if
20:  end if
21: end if
```

---

When the average of sensor *West* and *South* does not fall within 5%, the average of the measurements of sensor *North* is appended to the array. Subsequently, the array is sorted from low to high, and the highest and lowest value are removed. Lastly, the system will output the average of the truncated array if the average is within 5% moisture content. The system will indicate that no result is found if the measurements are not within any of the aforementioned bounds. This mostly happens when a sample contains physical damage and therefore will compromising the measurement, making it unusable.

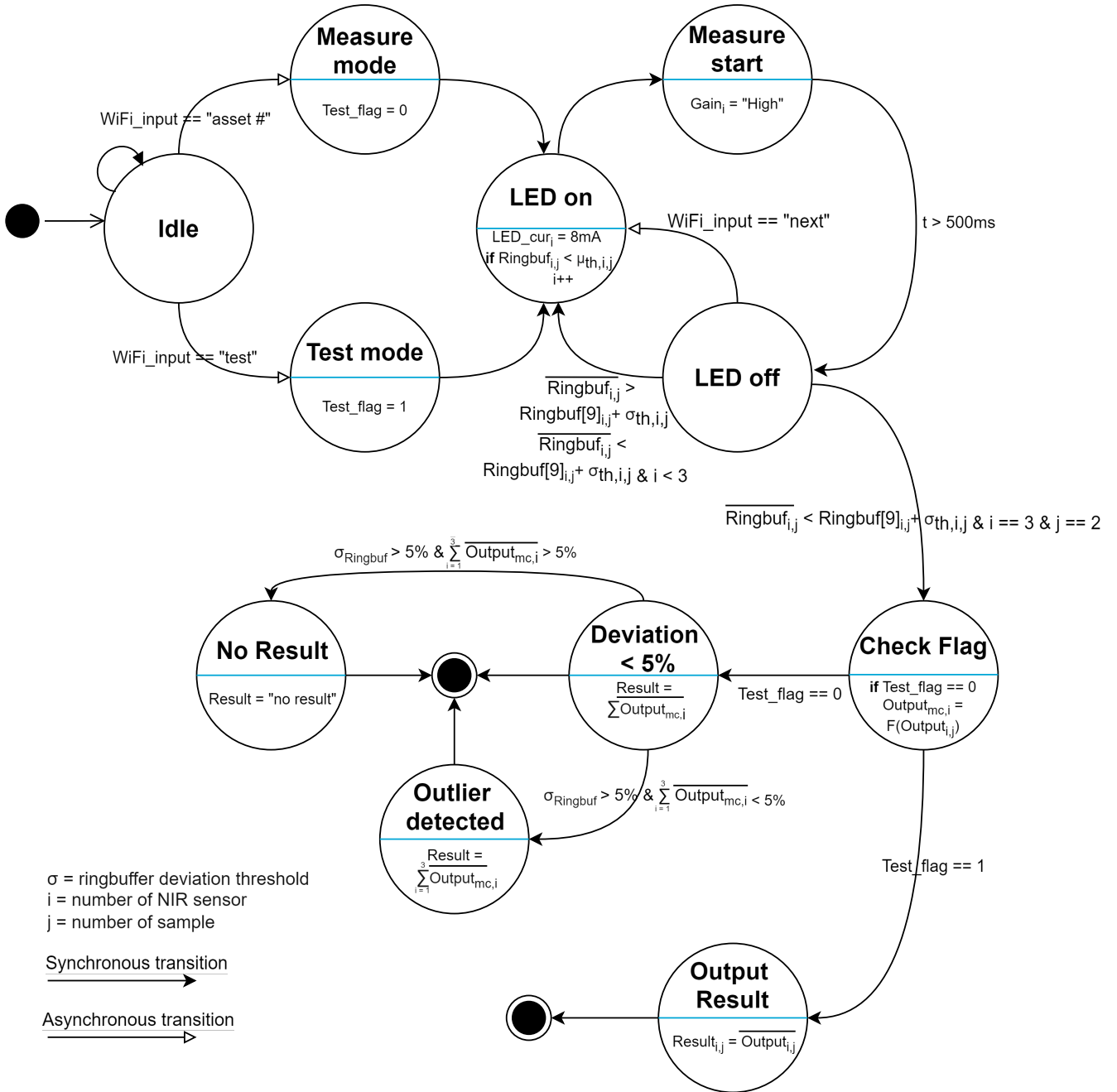


Figure 3.6: State machine representation of the internal functionality of the microcontroller. The order of the NIR sensors is dependent on the channels of the I<sup>2</sup>C Multiplexer, where *North* corresponds to  $i = 1$ , *East* to  $i = 2$ , *West* = 3, and *South* = 4.



## Chapter 4

# Experimental setup

In order to meet the discussed objectives in Section 2.4, an experimental setup must be designed and created. This setup must assure a uniform measuring environment under various conditions. Since the sensor measures light reflectance, it is important to block any stray light and have a flat and uniform holder to place the paper sample in such that each individual measurement provides a reproducible output. Additionally, the sensor must be configured in an optimal way such that clear differences in small amounts of moisture content can be measured. Finally, a testing procedure is proposed such that all measurements are performed similarly. This will ensure that the extracted moisture content estimation model from the performed tests will be accurate for all future measurements.

### 4.1 PILC paper sample holder

As described in Section 2.4, it is important to create an uniform measuring environment such that the measurements from the sensor will be reliable. The reliability of the sensor is dependent on various factors. The stray light or a different distance between the paper sample and the sensor could compromise the reproducibility of the measurements. This conclusion has been derived from preliminary testing, during which the P13567-02CT sensor was left uncovered and directly exposed to sunlight. This exposure led to an overflow in the sensor's output register. Given the inability to discern whether a measurement was compromised by sunlight or affected by non-uniform measuring distances, it becomes crucial to establish a measurement environment that entirely eliminates such influences.

Therefore, a 3D printed paper insulation sample holder was designed and created to ensure a reproducible output. The design and the dimensions of the sample holder can be seen in Figure 4.1. Here the dimensions of the sample holder were made in accordance with the dimensions of a standard microscope slide. In Figure 4.1, it can be seen that the insulation paper sample is placed between two microscope slides. This has been done in order to create an even surface for the paper sample to be laid upon. In addition, considering that the sensor operates based on light measurements, it was crucial to identify a material that would

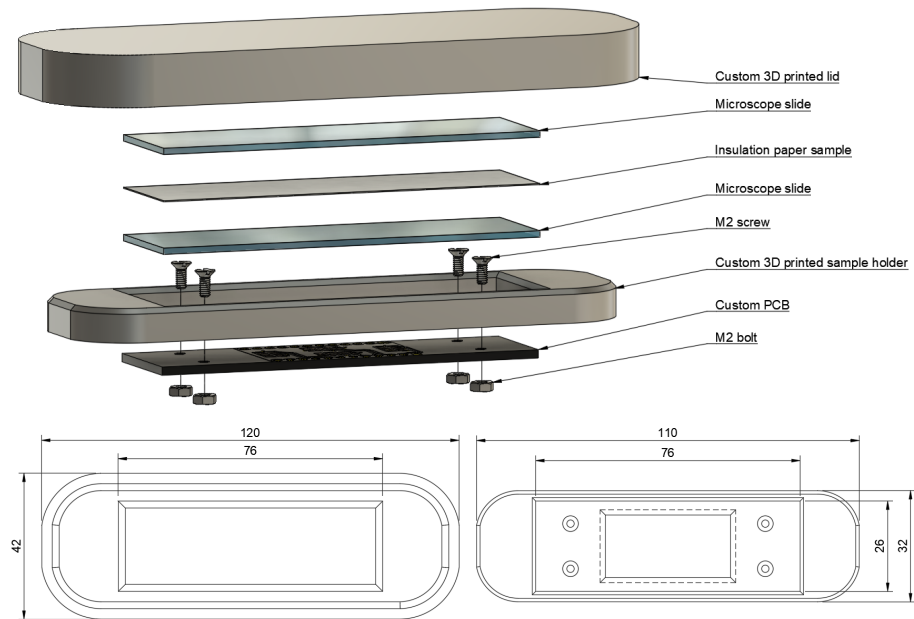


Figure 4.1: **The measuring setup consisting of a custom designed 3D printed sample holder, which can be screwed onto the created PCB, and a paper insulation sample between two microscope slides; Below that, the dimensions (in mm) of the 3D printed sample holder, with the lid on the left and the holder on the right.**

cause minimal interference with the light. Consequently, microscope slides were promptly selected as the most suitable material for this purpose. Furthermore, to further minimize any potential interference with the measurements, the 3D printed sample holder was intentionally designed in black, to decrease the effect of light reflection from the casing.

Additionally, since the paper insulation samples are wrapped around the conductor of the cable, the samples have a curvature when extracted from the PILC cable. This is due to the paper being in that same position for decades, making it almost impossible to straighten. A curved sample however is far from reliable when compared to another sample which undoubtedly has a different curvature. As a result, a second microscope slide is placed on top to fixate the paper in a flat position. Additionally, the lid has a protrusion designed in the middle. This protrusion pushes onto the microscope slide, guaranteeing that the paper sample is uniformly placed inside the sample holder.

Finally, to ensure that the measurement was conducted in a uniform and flat environment, the sample holder was specifically designed to be screw-mounted onto the custom PCB. This deliberate design choice effectively eliminates any deviations in the measuring distance, as it ensures that both components are securely maintained in a fixed position. The impact of the measuring distance will be further examined and discussed in more detail in Section 4.1.1.

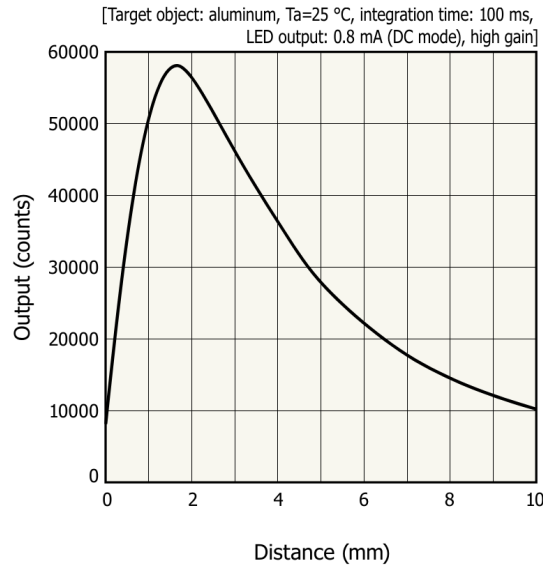


Figure 4.2: **Optimal sensor output with regards to distance between the sensor and the target object [23].**

#### 4.1.1 Measuring distance

The datasheet of the P13567-02CT specifies that the distance between the sensor and the target object has a significant influence on the resulting sensor output [23]. This is due to the scattering of the light emitted by the NIR LED. In Figure 4.2, the dependence between the sensor output and the distance between the sensor and the target object is shown. It becomes apparent that the sensor gives a maximum output for a distance of about 1.5 to 2.0 mm. This implies that this distance gives the most optimal scattering of the light from the LED. Using this distance between the paper insulation sample and the sensor limits any possible unwanted light reflectance. In order to ensure the paper insulation sample is placed at approximately this optimal distance, the sample holder has been made as thin as possible while still being structurally rigid. Consequently, the sample holder has been designed with a thickness of 1.0 mm, combined with the thickness of the microscope slide being 1.2 mm, the sample will have a fixed distance between measurements of approximately 2.2 mm to the sensor. This will result in a measuring distance close to the optimal sensor output.

## 4.2 Sensor configuration

Before a reliable model can be created from the measurement results of the P13567-02CT, the sensor needs to be configured properly. The P13567-02CT has multiple settings which can influence its output. This in turn will affect the sensitivity of the moisture estimation model. An evaluation of these settings with regards to the accuracy of the NIR measurement is critical in order to accurately model the sensor output to moisture measurements. An overview of the internal registers containing the sensor settings is shown in Table 4.1.

Table 4.1: The address map of the P13567-02CT, containing the settings of the sensor.

P13567-02CT									
Adrs		bit							
		7	6	5	4	3	2	1	0
00	Initial setting	Reset	Standby	Standby function monitor	Register reset	Gain	Integration mode	Integration time	
	Function	0: Operation 1: reset	0: Operation 1: Standby	Readout only	0: Reset release 1: Address 03-0A Data reset	0: High gain 1: Low gain	0: Fixed time mode 1: Manual setting mode	(00) 32 $\mu$ s (01) 0.5 ms (10) 8.2 ms (11) 65.5 ms	
0E	Initial setting	LED reset	LED standby	DC mode	1/10 mode				
	Function	0: Operation 1: reset	0: Operation 1: Standby	0: Pulse mode 1: DC mode	0: Normal mode 1: 1/10 mode				
0F	Initial setting	LED drive current							
	Function	0: 0 mA 1: 64 mA	0: 0 mA 1: 32 mA	0: 0 mA 1: 16 mA	0: 0 mA 1: 8 mA				

Six main settings can be found for the NIR sensor: gain, integration mode, integration time, DC/pulse mode, Normal/Low current mode, and the LED drive current. The settings regarding the gain and the LED drive current require a critical analysis and trade-offs. These two settings will be further discussed in Section 4.2.1. The remaining settings will be discussed below:

- **Integration mode:** The integration mode will determine the way the photodiode will measure. This means that the photodiode can be either set to measure for a fixed time, or the time it measures can manually be set, using the manual timing register. However, since the stabilization time of the sensor output is unknown, the sensor is configured in manual setting mode. Additionally, the manual setting mode will automatically set the sensor to sleep mode while the microcontroller processes the data, achieving a better energy efficiency [23].
- **Integration time:** The integration time will determine the duration of the measurement if the sensor is configured in fixed time mode. If the sensor is configured in manual setting mode, the manual timing register will determine the duration of the measurement. The manual timing register is left unchanged from its default value of 400 ms, since the stabilization time of the sensor output is unknown. Furthermore, the system is configured to take repeated measurements, as mentioned in Section 3.4.2, therefore the duration of a single measurement has little effect on the final result.
- **DC/Pulse mode:** This setting will determine whether the LED will be provided with a DC current or a pulsed current. There is no additional benefit in changing the LED current drive type, in order to make the LED repeatedly flash, in the proposed NIRS system. As a result, this setting is configured in DC mode.
- **Normal/Low current mode:** The low current setting will reduce the LED drive current set in the  $0F$  register by a factor of ten. Consequently, this setting is inherently connected to the LED drive current. Therefore, the configuration of this setting will be further discussed in Section 4.2.1.

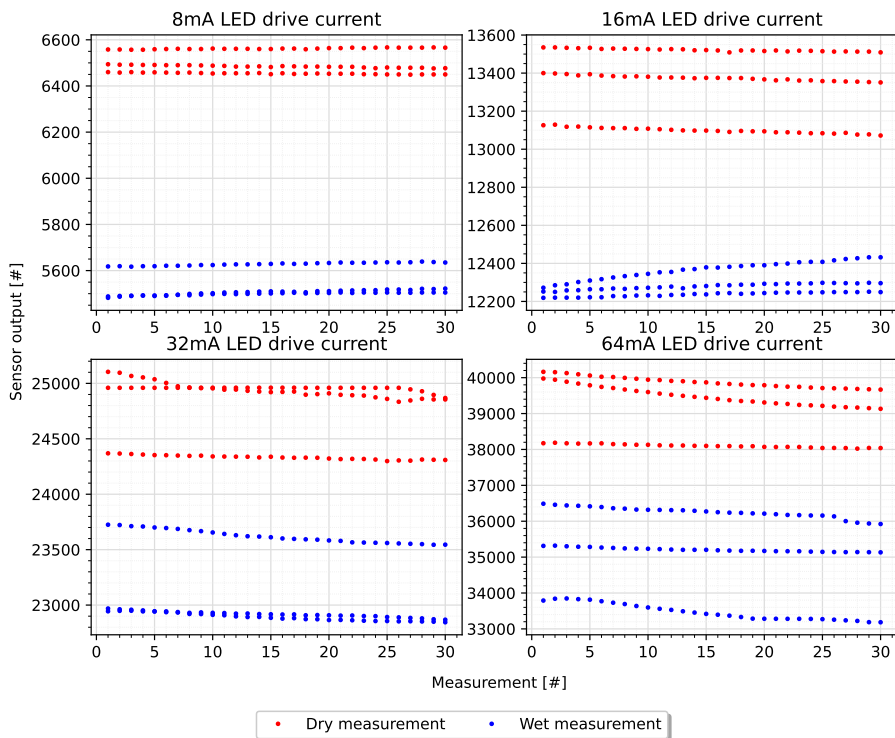


Figure 4.3: The effects of various LED drive currents on the sensor output for dry and wet samples.

#### 4.2.1 LED drive current and gain

Selecting the appropriate LED drive current and gain involves critical trade-offs. In order to limit power consumption in the system, a lower LED drive current is preferred. However, a lower LED drive current directly affects the intensity of light emitted by the LED, resulting in a lower sensor output. Since the resolution of the sensor is directly related to the smallest detectable change in moisture content of the measured sample, this in turn lowers the resolution of the result, which is an unwanted effect. Since it is expected that the moisture content of the measured samples could have minor differences, a high resolution can be critical in order to measure these small differences.

In contrast, a high gain is desirable, because it enhances the resolution of the sensor output. However, the reflectance of the sample has a significant impact on the gain. The output register of the sensor has a maximum size of 16 bits. A high gain system could result in the output register overflowing and compromising the measurement in the process. As a result, the challenge is to maximize the sensor output without causing an overflow in the output register. This requires the system to be calibrated on the sample to balance the LED drive current with the appropriate gain settings.

In Figure 4.3, the effects of various LED drive currents on the sensor output for dry and wet samples is shown. The wet paper samples have been soaked in water for approximately twenty minutes, such that a significant difference should be found in the sensor output between dry and wet measurements. All measurements were performed on a low gain setting, such that the output register would not overflow on the highest LED drive current setting.

Obviously the sensor output greatly increases when the LED drive current increases, as can be seen in Figure 4.3. The sensor output approximately doubles from a doubling of a low LED drive current. However, when comparing the 8 mA LED drive current to the 64 mA LED drive current, the sensor output only yields an approximate multiplication of around six, while the LED drive current has multiplied by a factor of eight. Therefore, a higher LED drive current leads to a larger scattering. This can be seen in the relative difference of the sensor output in *Counts* of dry and wet measurements at the different LED drive currents. While the relative difference of the sensor output between dry and wet measurements at 8 mA is approximately 1000 *Counts*, the difference at 64 mA is approximately 4000 *Counts*. This is a factor of only four times higher, while the LED drive current has multiplied by a factor of eight. Therefore, the lowest LED drive current provides the best distinguishable difference between wet and dry measurements.

As previously mentioned, a low LED drive current will result in a low resolution. However, as seen in Figure 4.3, the lowest LED drive current will result in the most reproducible results. Consequently, the gain setting will be configured to high gain, which increases the resolution. As a result, the current mode will also be configured to normal, since a low current mode will further reduce the resolution.

#### 4.2.2 Circular buffer

Preliminary testing showed that the sensor output showed variability over time. The sensor output requires time to stabilize to a steady-state output. Con-

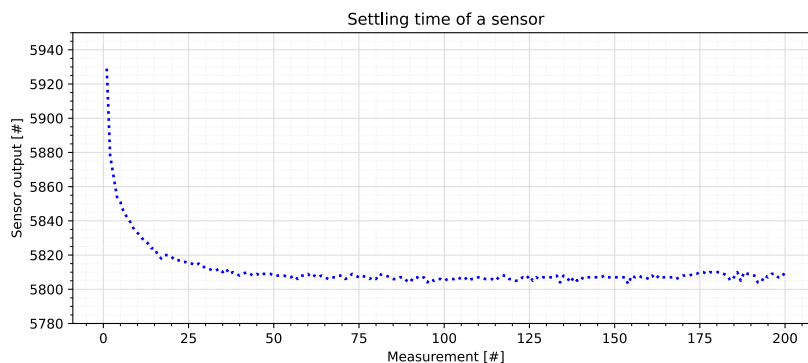


Figure 4.4: **The settling time of the sensor output of a measurement at 8 mA LED drive current and low gain.**

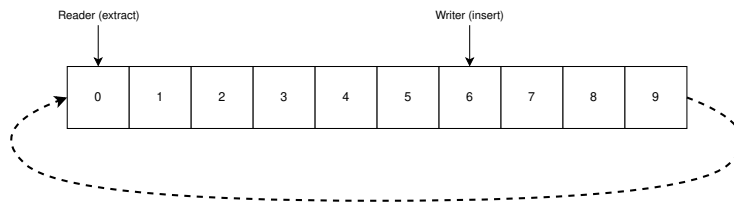


Figure 4.5: **Working principle of a circular buffer, where the reader and writer can move independently.**

sequently, a method had to be designed in order to avoid prematurely terminating the measurement cycle, as discussed in Section 3.4.2.

In Figure 4.4, the typical curve of the settling time is shown. It can be seen that the sensor output of an individual NIR sensor stabilizes between 50 and 100 measurements. It is hypothesized that the electrical components may need time to reach a stable operating temperature upon startup, which can affect their output. Moreover, it is important to highlight that the settling time is not consistent across different measurements. In fact, the settling time varied from one measurement cycle to another, suggesting that the settling process is inconsistent. This variability in settling time poses potential concerns in regards to when to terminate the system. If the system is terminated before the sensor has reached its steady-state output, a risk exists that the corresponding moisture content derived from the measurement could deviate from its true value. Consequently, this deviation could lead to inaccurate assessments. This could potentially be harmful for the reliability of the data collected and subsequent analyses based on these results.

A solution to address the issues with a variable settling time is to introduce a circular buffer. A graphical representation of a circular buffer is shown in Figure 4.5. A circular buffer is a data structure that stores a predetermined number of measurements in a fixed array over time. In a circular buffer, the writer and reader can move independently from one another. The writer will overwrite the oldest data as a new measurement is performed. By implementing a circular buffer, the system can store multiple measurements, enabling it to track the output of the sensor as it approaches its steady-state output. Additionally, it limits the amount of measurements saved in the memory.

The use of a circular buffer can increase the reliability of the sensor output in several ways. Firstly, by storing recent measurements, the system can determine when the output of the sensor has stabilized. This enables the system to identify the steady-state output of the sensor based on the contents of the circular buffer, in contrast to relying on a single measurement that may be influenced by fluctuations. Additionally, the circular buffer enables the system to filter the measurements. Namely, the output can be refined by taking the average of the measurements within the circular buffer. This can reduce the impact of potential fluctuations in the measurements and improve the accuracy of the sensor output.

The introduction of a circular buffer changes the operation of the software. Specifically, the transition between the sensors, as described in Section 3.4.2, changes based on the contents of the circular buffer. Now, only when the average of the measurements stored in the circular buffer is within a threshold of 5 *Counts* from the latest measurement, the system saves the latest measurement, and switches to the subsequent sensor. The threshold of 5 *Counts* is chosen due to the inherent deviation of the NIR sensor of up to 10 *Counts*, even when the LED is standby [23]. By continuously comparing the most recent measurements to the average of the circular buffer when it is added, the system can determine when the sensor output has stabilized. This ensures that the output of the sensor has stabilized in fact stabilized before terminating the measurement. This reduces the risk of prematurely switching that could lead to inaccurate results.

### 4.3 Testing procedure

In order to have reliable measurements and results, a standardized testing procedure is essential. A generic testing procedure ensures that all measurements are performed consistently, and improves the reliability of the collected data. Additionally, future measurements will only be meaningful if the same measurement procedure is applied as was used for the reference model proposed in Section 5.3.

As mentioned in Section 2.2.3, a reference method is needed in order to relate the moisture content of the paper insulation sample to the sensor output in *Counts* by the NIRS system. Therefore, the LOD method has been used to determine the moisture content of the paper insulation samples, as mentioned in Section 2.2.2. This method involves drying the paper insulation samples in an oven at 105°C for the duration of one to multiple hours [43].

Before oven drying, the paper insulation samples have to be accurately weighed. This has been done by making use of a VWR Classic precision balance. This balance can measure up to milligrams. Each paper sample had its resin removed and had a mass of roughly 1.5 g. Subsequently, the paper insulation samples were soaked in water for a predetermined hydration time. After which, measurements were made using the *North*, *West*, and *South* NIR sensors. After oven drying, the paper insulation samples are weighed again. The moisture content can be derived from the weight difference between the measurements [43]. At certain intervals the paper insulation samples were preliminarily weighed in order to determine the required drying duration before a steady state was achieved with regards to the moisture content of the paper insulation samples. It was determined that the weight of the paper insulation samples remained constant after one hour.

## 4.4 Cable information

The paper insulation samples used for the measurement results of Section 5.2 and Section 5.3, originate from a 3-core PILC cable with a aluminium conductor area of 150 mm<sup>2</sup>. An overview of the used cable can be found in Appendix C. While it is unsure how long the cable has been in operation, the cable tag within the cable showed it was manufactured in 1976. Consequently, the cable has probably been in operation for roughly 40 years. Due to the translucency difference between the insulation paper around the conductor and the paper within the cable belt, a direct comparison between the two types of paper is impossible. In Figure 1.1, the two types of insulation paper can be seen. At the indication of paper insulation, the insulation paper around the conductor can be seen on the left, and the paper insulation of the cable belt can be seen on the right. The insulation paper from the cable belt is used for measurements, since the paper around the conductor is too small to fit inside the sample holder, and more paper is available from the cable belt. A PILC cable consists of 12 belt paper layers. All layers except the first and the last were used in the measurements, where each paper layer was used for a different hydration time.



## Chapter 5

# Results and Discussion

One of the in Section 2.4 mentioned objectives is the creation of a model which is able to relate the NIR-sensor output to the moisture content of the paper insulation samples. This chapter will describe the results found in order to create this model by making use of the methods described in Section 4.3. It is found that this method was not as reliable as anticipated. The resin found on the paper insulation samples had a significant impact on the resulting measurements, and therefore had to be removed in order to gain reliable results. The results found during testing which included the resin can be found in Section 5.1. In addition, it is found that the sensitivity of the system to outliers is significant. This further proves the need for an outlier removal algorithm, as proposed in Section 3.4.4. Lastly, by making use of the updated measurement procedure the results with and without making use of the outlier removal algorithm are compared. This resulted in a reduction from approximately  $\pm 3\%$  moisture content deviation from the reference model, as shown in (5.3), to a deviation of approximately  $\pm 1\%$  moisture content from the reference model.

### 5.1 Resin effect

The PILC paper insulation samples were prepared for testing as described in Section 4.3. However, it became clear that the proposed method had its drawbacks. As seen in Figure 5.1, the data shows no clear correlation. This was caused by the resin still being present on the paper insulation samples. Namely, in Figure 5.1, the NIR sensor output of measurements where the resin was still present on the sample are shown. For each hydration time, three different paper sample measurements were taken. However, no clear correlation could be found between the NIR sensor output and hydration time for either of the three different NIR sensors. The data points differ significantly, even on really similar hydration times. Therefore, a reliable model could not be extracted from this data, and a different sample preparation method was needed.

During testing it was also found that physical blemishes on the sample would result in unreliable data. This was likely caused by the light from the emitted by the LED being unpredictably scattered within the enclosed measuring environment. This suspicion was further proven by the fact that the measure-

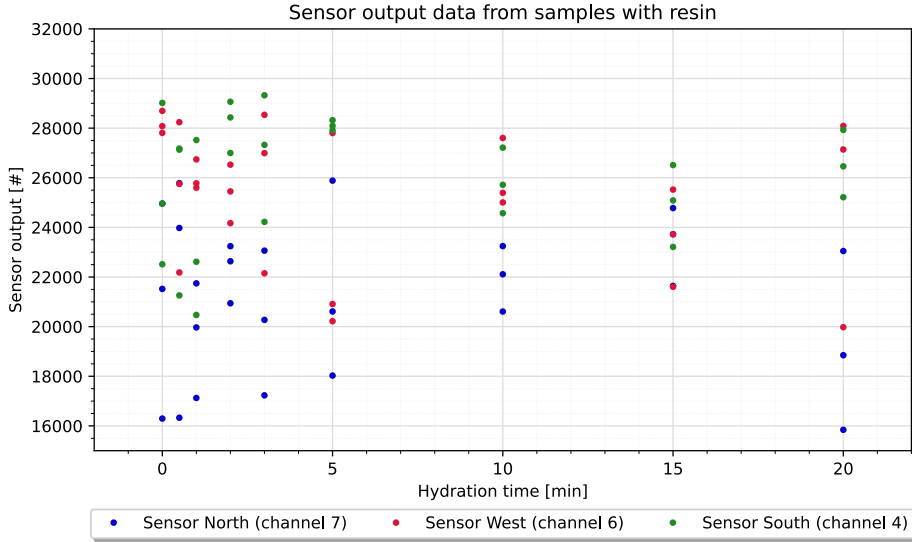


Figure 5.1: **Sensor output against hydration time from samples where the resin is still present. Three paper samples were used per hydration time.**

ments with the resin present on the samples also resulted in uncorrelated data as shown in Figure 5.1. The resin is uniformly applied on the paper insulation during manufacturing, however during years of operation the resin is able to redistribute. Temperature and elevation cause the resin to migrate and form clumps. Light from the LED will scatter when it comes in contact with these clumps. As a result the light will again have an unpredictable scatter when the resin is not removed from the sample, resulting in uncorrelated data.

## 5.2 Hydration curve

By making use of the testing procedure as described in Section 4.3, the hydration data as seen in Figure 5.2 was found. The data follows an exponential saturation curve. Which is expected since the paper insulation would reach its hydration saturation over time. Therefore the data was fitted with an exponential saturation formula:

$$M_c = C_h - R_h \cdot e^{-k_h \cdot t_h}, \quad (5.1)$$

where  $t_h$  represents the hydration time in minutes and  $k_h$  the saturation rate, which is dimensionless. The remaining variables are all in percentages, where  $M_c$  represents the moisture content,  $C_h$  the moisture saturation, and  $R_h$  scales  $M_c - C_h$  to the initial moisture content of the samples. All variables are denoted using four significant figures, since the scientific scale used to determine the moisture content had the same accuracy.

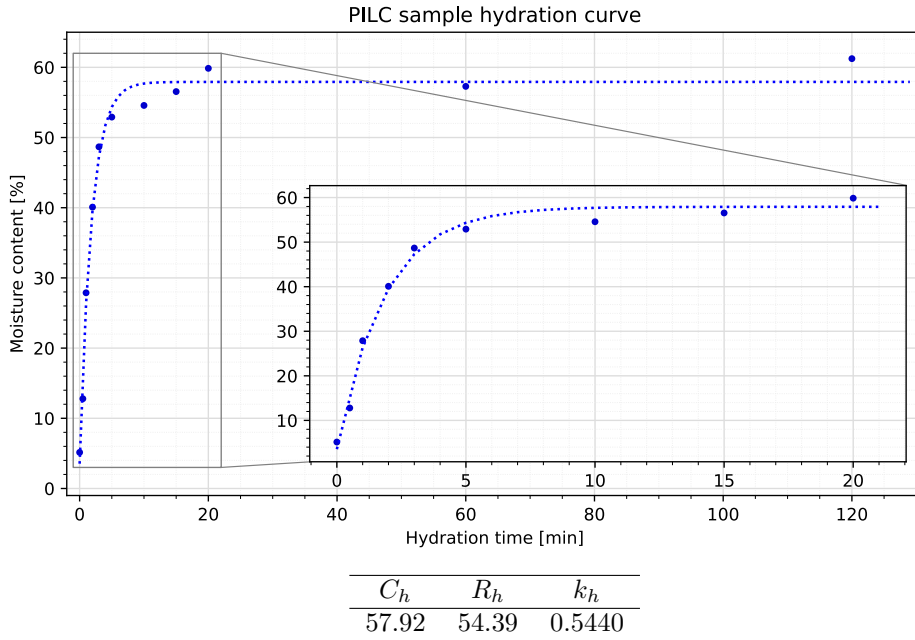
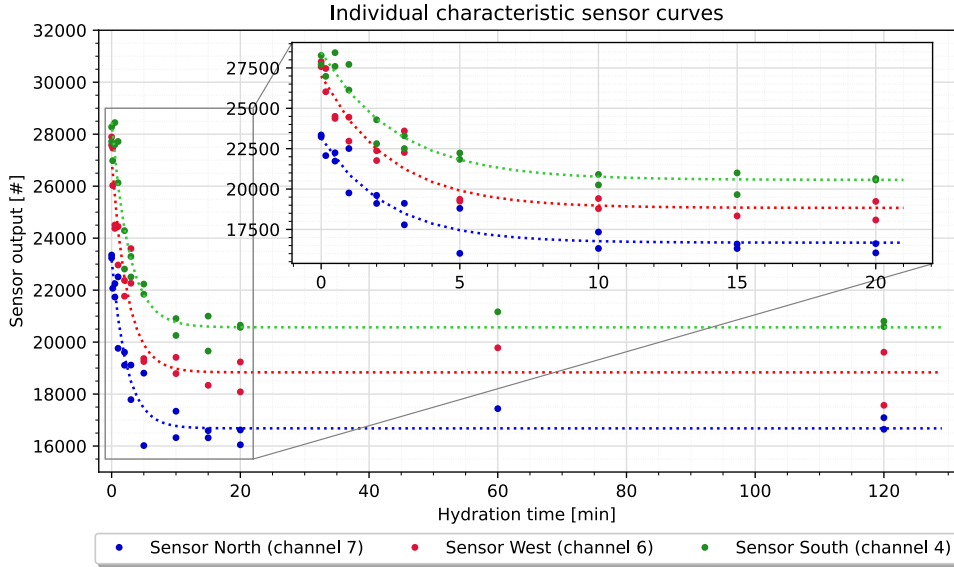


Figure 5.2: Moisture absorption of one PILC paper insulation sample per hydration time, plotted over hydration time with the resin removed from the samples and the parameters associated with the fitted exponential saturation curve. One paper samples was used per hydration time.

A clear trend was found between hydration time and moisture content of the paper insulation sample. However, small deviations from this exponential trend were present in the collected data. Due to the nature of the results, a small deviation between the measurement and reality could potentially be problematic, since a few percentages difference in moisture content could lead to wrong decision making. While the model needs further refinement in order to ensure reliable results with regards to cable deterioration based on the moisture content of the PILC cable insulation, a small inaccuracy will still yield objectively better results compared to the original method of dropping the insulation in a tub of oil.

The moisture absorption as seen in Figure 5.2 varies from 0% to approximately 60%. This is not comparable to a paper sample extracted from a PILC cable in operation, which still includes the resin. The non-polar resin slows the absorption of water in the paper insulation sample due to its hydrophobic nature. As a result, the hydration curve rises to moisture contents which will not be found in cables in operation. While this does not pose issues within the system design, since the sensor outputs are calibrated against the same samples, it is important to note that the hydration curve reaches higher moisture content than cables can reach in operation. This suggests that the system is calibrated against a situation which is not necessarily a representation of reality. Therefore more measurements are needed within the moisture content range of 0% to 20%.



Sensor	$C_s$	$R_s$	$k_s$
North	16680	6471	0.4252
West	18835	8167	0.4063
South	20568	7886	0.3697

Figure 5.3: Sensor output corresponding to two PILC paper insulation samples per hydration time with the resin removed and the parameters associated with the fitted exponential curve from (5.2). Two paper samples were used per hydration time.

### 5.3 Sensor characteristics

In Figure 5.3, the sensor outputs corresponding to the same samples and hydration times as in Figure 5.2 are shown. For each hydration time, two measurements per NIR-sensor were conducted. One paper insulation sample contained some physical damage which greatly impacted the fitted trend and therefore was omitted from this model. The omitted sample was a measurement of 60 minutes hydration time. The NIR sensor output in *Counts* were 22947, 24711 and 23651 for the NIR sensors *North*, *West*, and *South* respectively. In contrast, the second measurement at 60 minutes hydration time showed an NIR sensor output of 17438, 19780, and 21165 for the NIR sensors *North*, *West*, and *South* respectively. The moisture saturation of the sample is achieved long before this time stamp, as can be seen in Figure 5.3. Therefore, removing this data point will have negligible impact on the model.

A linear relation is expected between the moisture content of the paper insulation and the sensor output, therefore the sensor output data was expected to have an inverse exponential trend in comparison to (5.1):

$$Output = C_s + R_s \cdot e^{-k_s \cdot t_h}, \quad (5.2)$$

where *Output* corresponds to the raw NIR sensor output in *Counts* and  $t_h$  corresponds to the hydration time in minutes. The remaining variables are all dimensionless, where  $C_s$  represents the sensor output in *Counts* as the paper sample reaches saturation,  $k_s$  represents the saturation rate, and  $R_s$  scales  $Counts - C_s$  to the initial sensor output for a paper insulation sample of zero hydration time.  $C_s$  and  $R_s$  are denoted in integers, since the NIR sensor rounds to the nearest integer. Additionally,  $k_s$  is denoted using four significant figures, since the scientific scale used to determine the moisture content had the same accuracy.

The data points show a clear exponential trend with deviations from the trend at all hydration times. This further confirms the suspicion that the NIRS system is prone to outliers, as earlier discussed in Section 3.4.4.

The extrapolated exponential trend was subsequently combined with the hydration curve as extrapolated from Figure 5.2. This resulted in the moisture curve per sensor, as seen in Figure 5.4, which shows the moisture content for each sensor output. As mentioned previously, a lot of data points are at moisture contents of above 20%. A moisture content that high is artificial and will seldom be encountered from cables which have naturally aged in the field. This means that the fitted curve should be fitted more towards the lower end of the moisture spectrum. When fitting the data with an inverse linear regression, the data would more accurately represent the higher moisture range, since more data points are available within this range. As a result, an inverse regression would not accurately represent the lower end of the moisture spectrum, where the most important data lies. From Figure 5.4, the data suggests that, at the lower end of the moisture spectrum, the trend seems to follow an inverse linear regression, however not enough data has been gathered in this region to support this claim yet. Thus, the fitted curve was chosen as a second degree polynomial instead of a inverse regression which was initially anticipated upon:

$$M_c = -A \cdot Output^2 + B \cdot Output + C, \quad (5.3)$$

where  $M_c$  represents the moisture content in percentages and *Output* represents the raw NIR sensor output in *Counts*. The variables,  $A$ ,  $B$  and  $C$  act as the multiplier for determining the shape, orientation and position of the second degree polynomial,  $A$  is in percentages per  $Counts^2$ ,  $B$  is in percentages per *Counts*, and  $C$  in percentages.

What becomes apparent is that the curves per NIR sensor do not appear identical. A horizontal offset could be expected due to the sensor not being completely identical. Additionally, the curve from the *North* sensor seems to have a different trajectory in comparison to the other two sensors. This could be due to some physical damage to the top epoxy layer of the sensor, causing the measurements to somewhat skew. However, also the slope of the polynomial trends, denoted by  $B$ , of the other two sensors are slightly different. This suggests that each individual sensor reacts slightly differently to a change in moisture content of the measured sample.

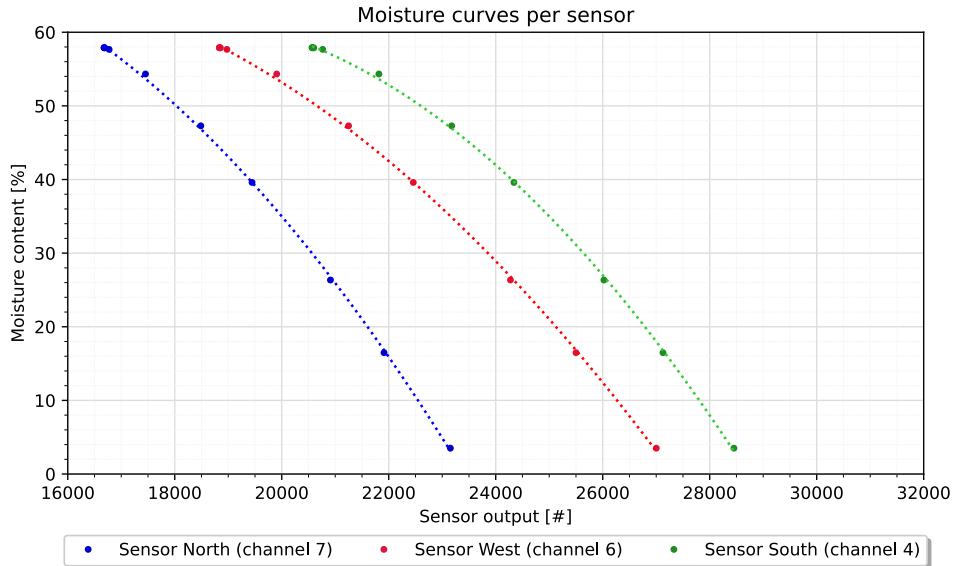


Figure 5.4: The fitted curve of the sensor output plotted against the fitted curve of the moisture absorption of a PILC sample and the parameters associated with the fitted second degree polynomial as seen in (5.3).

It is important to state that deviations in the slope of the model per individual sensors exist in the current model. While this is unlikely, it is possible that differences caused by manufacturing exist between sensors, it is however more likely that these small deviations stem from measuring inaccuracies. Further testing needs to be done to prove whether these deviations are caused by the manufacturing process, the system assembly, or simply by inaccuracies in the model which were explored previously.

## 5.4 Effects of outlier removal algorithm

The sensor output data shows a clear inverse exponential trend, as seen in Figure 5.3, however deviations from the trend were found at all hydration times. Some deviations were minor, however also somewhat substantial deviations were also found. This suggests that the NIRS system is prone to outliers. These outliers could potentially disturb the final results if they are not caught. Additionally, the user has no reference to judge the final results on, therefore are unable to catch the outlier themselves. While the data shows a very clear trend, the outliers could potentially have ruinous effect on the reliability of the sensor

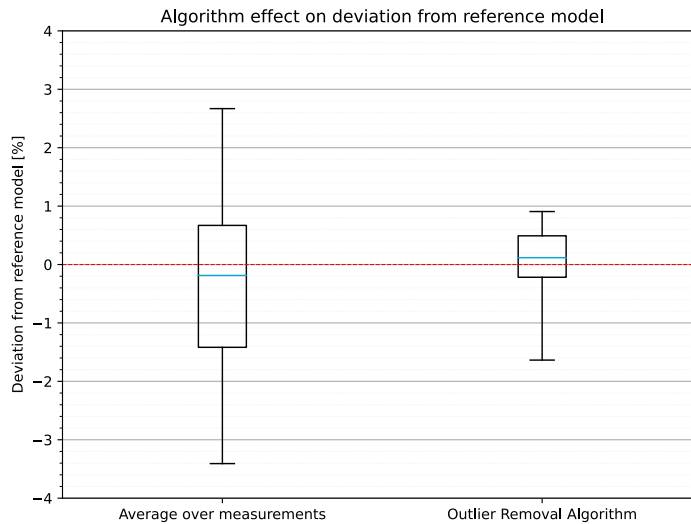


Figure 5.5: **The effect of the outlier removal algorithm on the deviation from the reference model, constructed of one moisture content measurement per hydration time.**

itself. Therefore, an on-chip outlier detection algorithm was introduced. In Section 3.4.4, the functionality of the outlier detection algorithm is thoroughly explained.

By making use of the algorithm as the described in Algorithm 1, a reduction in deviation of moisture content from the reference model, proposed by Equation 5.3, was found. This can be seen in Figure 5.5. This means that the outlier removal algorithm is successful in removing outliers and increasing the accuracy of the system with regards to the moisture content of the paper insulation sample. Additionally, it proves that even a sensor which has been damaged can still serve a very useful purpose. Sensor *North* has proven to be successful in reducing the deviation from the reference model and improving the reliability of the system. This is important to note due to the relatively high cost of the sensor in comparison to the total system. While more data is needed to determine the exact sensitivity of the system, the algorithm has proven to be effective in increasing the reliability while being having low computational intensity.



## Chapter 6

# Conclusions

The proposed NIRS system performs measurements on one particular absorption band of water; the absorption band around 1450 nm. This wavelength is selected due to its high absorption coefficient and the availability of cost-effective photodiodes in this wavelength range. Due to the many advantages, like digital communication and an optimized LED and photodiode in a single package, the P13567-02CT NIR sensor is selected as the NIRS component. A custom PCB has been designed and manufactured in order to accommodate for the custom package of the P13567-02CT NIR sensor. This PCB has been designed to fit four P13567-02CT NIR sensors in order to average out measurement fluctuations. The measurements of the P13567-02CT NIR sensor are processed by an Arduino Nano 33 IoT. The NIRS system is initiated through the cloud connection of the Arduino Nano 33 IoT. Additionally, the final measurement results are uploaded to the cloud.

Additionally, the external influences to a NIRS measurement were examined, and a measuring setup is proposed which limits the effects of external influences on the measurement results. Additionally, a testing procedure is proposed which ensures that future measurements are performed consistently, and enables the further development of the NIRS system. It was found that the resin on the paper insulation samples had a significant impact on the measurement results. Consequently the measurements were performed on paper samples where the resin was removed. As expected, a linear relation was found between the P13567-02CT NIR sensor output and the moisture content at moisture contents of 0% to 20%. However, additional measurements are still needed within the range of 0% to 20% moisture content of the paper samples to validate this.

The proposed NIRS system achieves the theoretical accuracy of  $\pm 1\%$  by making use of the presented outlier detection algorithm which is able to increase the accuracy of the NIRS system from  $\pm 3\%$  to  $\pm 1\%$ , by removing outliers of individual NIR sensors and averaging the results of multiple measurements. However, the model as seen in Equation 5.3 requires further refinement, and additional measurements need to be performed in order to verify the accuracy. The final measurement results of the NIRS system is linked to the asset number of the PILC cable under test, and uploaded to the cloud to enable further data analysis. All in all, this research has laid the groundwork for moisture

measurements on PILC cables.

## Chapter 7

# Future Work

In order to improve on the presented NIRS system and provide additional research directions, recommendations are presented for future work. Some recommendations include additional analysis on the current implemented system as well as the continuation of experiments in order to obtain more data and refine the existing models. The following recommendations aim to guide future work towards enhancing the capabilities and applications of the NIRS system in monitoring the condition of PILC cables:

- To enhance the accuracy of the NIRS system, it is crucial to obtain more data points in the lower range of moisture content, namely from 0% to 20%. Current models may not accurately reflect the moisture content of cables in operation. Increasing the number of measurements in this range will allow for the models to more precisely reflect cables in operation.
- As more PILC cables are analyzed using the NIRS system, a dataset can be established of all measured PILC cables. This dataset can be utilized to develop a machine learning model capable of predicting the moisture content of PILC cables based on key indicators, like age, cable loading and the type of soil the cable is in. By extrapolating from the analyzed sample data to the wider population of PILC cables, this model could predict the moisture content and provide valuable insights into the expected lifespan of these assets, aiding in maintenance and replacement decisions.
- Developing a NIRS system capable of simultaneously measuring multiple samples could improve the data collection efficiency, as well as the system accuracy through better detection of outliers and more robust data analysis. Although the relative high cost of the NIR sensors is a consideration, the development of such a system could improve the moisture content estimation.
- Instead of uploading the results of the NIRS system to an external cloud, the results could be uploaded to the database of Alliander. Integrating the NIRS system with the already existing database of Alliander would allow for automatic updates to the PILC cable records with additional information, which would streamline data management.

- Given the challenges of monitoring the moisture content from the insulation paper while the cable is still in operation, an alternative strategy could involve assessing the hardness of the lead sheath. Some studies suggest a correlation between the hardness of the lead sheath and its age. As the lead sheath serves as a protective barrier for the cable insulation, online monitoring of its hardness could provide indirect insights about the condition of the insulation paper underneath. Further research is required to validate this method, and develop new monitoring techniques.

# Bibliography

- [1] Arduino. *Arduino Due Product Reference Manual*. 1st edition, 2024.
- [2] Arduino. *Arduino Nano 33 IoT Product Reference Manual*. 1st edition, 2024.
- [3] Arduino. *Arduino Uno R4 WiFi Product Reference Manual*. 1st edition, 2024.
- [4] A. Barth. *Molecular Vibrations and Their Interaction with Electromagnetic Radiation*. Springer Berlin Heidelberg, 1st edition, 2013.
- [5] P. Carlini, R. Massantini, and F. Mencarelli. Vis-nir measurement of soluble solids in cherry and apricot by pls regression and wavelength selection. *Journal of Agricultural and Food Chemistry*, 48(11):5236–5242, 2000.
- [6] CIGRE. Life management techniques for power transformers. *Power transformers and reactors*, 1(227), 2003.
- [7] CIGRE. Ageing of cellulose in mineral oil insulated transformers. *Materials and emerging test techniques*, 1(323), 2007.
- [8] CIGRE. Thermal performance of transformers. *Power transformers and reactors*, 1(393), 2009.
- [9] J. A. Conesa, J. A. Caballero, A. Marcilla, and R. Font. Analysis of different kinetic models in the dynamic pyrolysis of cellulose. *Thermochimica Acta*, 254(1):175–192, 1995.
- [10] J.P. Crine, V. Buchholz, M. Colwell, S. Cherukupalli, and B.S. Bernstein. Influence of aging on polarization currents and return voltage measured in PILC cables. *Conference on Electrical Insulation and Dielectric Phenomena*, 1(1):188–191, 2001-10.
- [11] Y. Cui, X. Li, L. Zhu, S. Ji, and F. Zhang. Research on influence of mechanical stress on insulation characteristics of oil-immersed pressboard. *2018 IEEE International Power Modulator and High Voltage Conference*, 1:264–268, 2018.
- [12] J. A. Curcio and C. C. Petty. The near infrared absorption spectrum of liquid water. *J. Opt. Soc. Am.*, 41(5):302–304, 1951.
- [13] J. Densley. Ageing mechanisms and diagnostics for power cables - an overview. *IEEE Electrical Insulation Magazine*, 17(1):14–22, 2001.

- [14] A. Deshpande, S. Deshpande, and S. Dhande. Nir spectroscopy based milk classification and purity prediction. *2021 IEEE Pune Section International Conference (PuneCon)*, pages 1–5, 2021.
- [15] J. Kuffel E. Kuffel, W.S. Zaengl. *High Voltage Engineering Fundamentals*. Newnes, 2nd edition, 2000.
- [16] A Ekenstam. The behaviour of cellulose in mineral acid solutions: kinetic study of the decomposition of cellulose in acid solutions. *BER*, 69:553, 1936.
- [17] A.M. Emsley and G.C. Stevens. Review of chemical indicators of degradation of cellulosic electrical paper insulation in oil-filled transformers. *IEEE Proceedings - Science, Measurement and Technology*, 141(5):324–334, 1994.
- [18] D.Y. Feng, Z.D. Wang, and P. Jarman. Modeling thermal life expectancy of the uk transmission power transformers. *2012 International Conference on High Voltage Engineering and Application*, 1(1):540–543, 2012.
- [19] The Electricity Forum. *Wire and cable and Wiring Methods Handbook*. 3th edition, 2007.
- [20] Antihus Hernández Gómez, Yong He, and Annia García Pereira. Non-destructive measurement of acidity, soluble solids and firmness of satsuma mandarin using vis/NIR-spectroscopy techniques. *Journal of Food Engineering*, 77(2):313–319, 2006.
- [21] K. D. Hakkel. Integrated near-infrared spectral sensing. *Nature Communications*, 13(1):103, 2022.
- [22] H. S. A. Halim and P. Ghosh. Condition assessment of medium voltage underground pvc cables using partial discharge mapping and polarization index test results. *Conference Record of the 2008 IEEE International Symposium on Electrical Insulation*, 1(1):32–35, 2008.
- [23] Hamamatsu. *Near infrared/proximity type sensor P13567-02CT*. 1st edition, 2024.
- [24] D.J.T. Hill, T.T. Le, M. Darveniza, and T. Saha. A study of the degradation of cellulosic insulation materials in a power transformer. part iii: Degradation products of cellulose insulation paper. *Polymer Degradation and Stability*, 51(2):211–218, 1996.
- [25] H. F. Holtzclaw, W. R. Robinson, and Nebergall W. H. *General Chemistry*. D.C. Heath, Lexington, Mass, 7th edition, 1984.
- [26] L. Huang, Y. Wang, X. Li, C. Wei, and Y. Lu. Effect of moisture on breakdown strength of oil-paper insulation under different voltage types. *2018 IEEE International Conference on High Voltage Engineering and Application (ICHVE)*, 1:1–4, 2018.
- [27] R. I. R. Javier, A. O. Baloloy, N. B. Linsangan, and I. V. Villamor. Portable non-invasive glucometer using near-infrared sensor and raspberry pi. *2020 4rd International Conference on Electrical, Telecommunication and Computer Engineering (ELTICOM)*, pages 35–39, 2020.

- [28] B. S. C. Kapali, Keerthika J, B. M. Lakshmi, and V. Swetha. Identification of blood glucose level using NIR sensor non-invasively. *2023 International Conference on Next Generation Electronics (NEleX)*, pages 1–4, 2023.
- [29] P. Klomklao, S. Kuntinugunetanon, and W. Wongkokua. Moisture content measurement in paddy. *Journal of Physics: Conference Series*, 901(1):012068, 2017.
- [30] H. Krässig and J.Schurz. *Cellulose*. John Wiley & Sons, Ltd, 1st edition, 2004.
- [31] N. Lelekakis, D. Martin, and J. Wijaya. Ageing rate of paper insulation used in power transformers part 1: Oil/paper system with low oxygen concentration. *IEEE Transactions on Dielectrics and Electrical Insulation*, 19(6):1999–2008, 2012.
- [32] S. Levchik, J. Scheirs, G. Camino, W. Tumiatti, and M. Avidano. Depolymerization processes in the thermal degradation of cellulosic paper insulation in electrical transformers. *Polymer Degradation and Stability*, 61(3):507–511, 1998.
- [33] X. Li and C. Li. Research on non-invasive glucose concentration measurement by nir transmission. *2015 IEEE International Conference on Computer and Communications (ICCC)*, 1:223–228, 2015.
- [34] Liander. *W7502 Werkinstructie montage MS-garnituren*. 1st edition, 2023.
- [35] Raspberry Pi Ltd. *RP2040 Datasheet A microcontroller by Raspberry Pi*. 1st edition, 2024.
- [36] R. D. Medina, A. A. Romero, E. E. Mombello, and G. Rattá. Assessing degradation of power transformer solid insulation considering thermal stress and moisture variation. *Electric Power Systems Research*, 151(1):1–11, 2017.
- [37] Y. Ozaki and Y. Morisawa. *Principles and Characteristics of NIR Spectroscopy*. Springer Singapore, 1st edition, 2021.
- [38] H. Peng, M. Dong, X. Wu, and Y. Liu. Identify moisture distribution in multilayer oil-immersed paper by frequency domain spectroscopy. *2012 IEEE International Conference on Condition Monitoring and Diagnosis*, 1:1130–1133, 2012.
- [39] N. Permal, C. K. Chakrabarty, A. R. Avinash, T. Marie, and H. S. A. Halim. Tangent delta extraction of cable joints for aged 11kv underground cable system. *2016 International Conference on Advances in Electrical, Electronic and Systems Engineering (ICAEES)*, 1:265–270, 2016.
- [40] A. K. Burnham R. Capart, L. Khezami. Assessment of various kinetic models for the pyrolysis of a microgranular cellulose. *Thermochimica Acta*, 417(1):79–89, 2004.
- [41] P. Samyn. Wetting and hydrophobic modification of cellulose surfaces for paper applications. *Journal of Materials Science*, 48(19):6455–6498, 2013.

- [42] D. H. Schroff and A.W. Stannett. A review of paper aging in power transformers. *IEE Proceedings C (Generation, Transmission and Distribution)*, 132(6):312–319, 1985.
- [43] M. Schubnell, C. De Caro, and R. Kunz. Moisture content, water content, loss on drying - part 1: What exactly is meant and how are these quantities determined? *Thermal Analysis UserCom*, 1(51):1–8, 2020.
- [44] K. Schöffski and D. Strohm. Karl fischer moisture determination. In *Encyclopedia of Analytical Chemistry*, volume 1, pages 1–13, 2006.
- [45] A Sharples. Degradation of cellulose and its derivatives. a. acid hydrolysis and alcoholysis. *Cellulose and cellulose derivatives*, 5(1):991–1006, 1971.
- [46] A. Shrotri, H. Kobayashi, and A. Fukuoka. Cellulose depolymerization over heterogeneous catalysts. *Accounts of Chemical Research*, 51(3):761–768, 2018.
- [47] K. T. Sithara Surendran and T. Sasikala. Sensor system based non-invasive system to measure glucose level in human body. *2019 3rd International Conference on Computing Methodologies and Communication (ICCMC)*, pages 203–207, 2019.
- [48] F. Steennis, P. Soepboer, J. Mosterd, P. Buys, P. Oosterlee, L. Bokma, and R. Meier. The effect of high current loads on joints in mv cable systems. *21st International Conference on Electricity Distribution*, 1(884), 2011.
- [49] B. Steuer, H. Schulz, and E. Läger. Classification and analysis of citrus oils by nir spectroscopy. *Food Chemistry*, 72(1):113–117, 2001.
- [50] J. Sugiyama. Visualization of sugar content in the flesh of a melon by near-infrared imaging. *J Agric Food Chem.*, 47(7):2715–2718, 1999.
- [51] Expressif Systems. *ESP32 Technical Reference Manual*. 1st edition, 2024.
- [52] H. Nambu T. Kashiwagi. Global kinetic constants for thermal oxidative degradation of a cellulosic paper. *Combustion and Flame*, 88(3-4):345–368, 1992.
- [53] Phase to Phase B.V. *Netten voor distributie van elektriciteit*. 5th edition, 2011.
- [54] J. Trygg, P. Trivedi, and P. Fardim. Controller depolymerisation of cellulose to a given degree of polymerisation. *Cellulose Chemistry and Technology*, 50:5–6, 2016.
- [55] S. Tsuchikawa, T. Ma, and T. Inagaki. Application of near-infrared spectroscopy to agriculture and forestry. *Analytical Sciences*, 38(4):635–642, 2022.
- [56] Y. Uchiho, Y. Goto, M. Kamahori, and K. Koda. New baseline correction method using near-infrared absorption of water in water/acetonitrile gradient high-performance liquid chromatography with far-ultraviolet absorbance detection. *Chromatographia*, 80(2):329–333, 2017.

- [57] A. Uhr-Müller, C. Weindl, B. Tepsäe, and K. Foit. Comparison of dielectric factors at different temperatures for new and pre-aged pilc cables. *2022 International Conference on Diagnostics in Electrical Engineering (Diagnostics)*, 1:1–4, 2022.
- [58] P. Williams. Karl h. norris, the father of near-infrared spectroscopy. *NIR news*, 30(7):25–27, 2019.
- [59] G. Xia and G. Wu. Study on the impact of initial moisture contents on ageing characteristics of transformer oil-paper insulation. *2016 IEEE International Conference on High Voltage Engineering and Application (ICHVE)*, 1(1):1–4, 2016.
- [60] M. Zapf, T. Blenk, A. Müller, H. Pengg, I. Mladenovic, and C. Weindl. Lifetime assessment of pilc cables with regard to thermal aging based on a medium voltage distribution network benchmark and representative load scenarios in the course of the expansion of distributed energy resources. *Energies*, 14(2), 2021.
- [61] J. Zhang, Y. Jiao, Q. Chen, L. Zhou, H. Li, and Y. Tong. An online measuring method for tangent delta of power cables based on an injected very-low-frequency signal. *IEEE Sensors Journal*, 22(1):980–988, 2022.
- [62] S. Zvanovec, P. Chvojka, P. Haigh, and Z. Ghassemlooy. Visible light communications towards 5g. *Radioengineering*, 24(1):1–9, 2015.



## Appendix A

### NIRS system overview

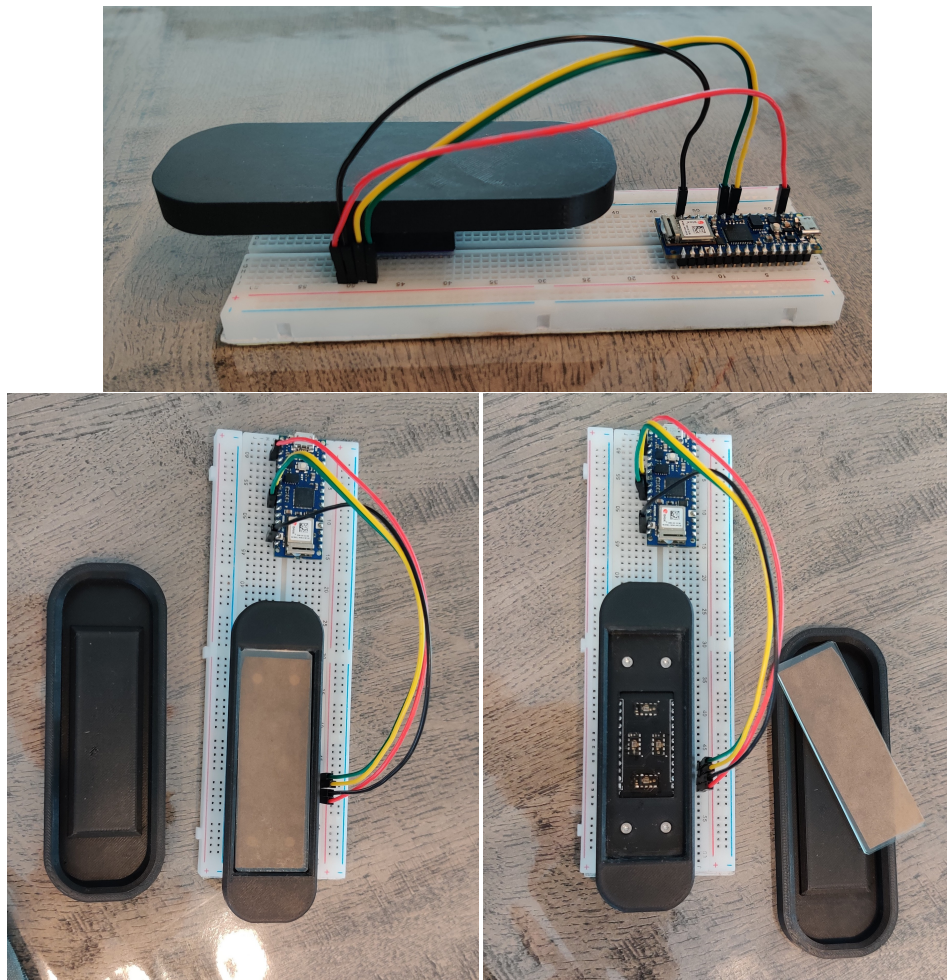


Figure A.1: Overview of the NIRS system with an insulation sample.

# Appendix B

## PCB schematic

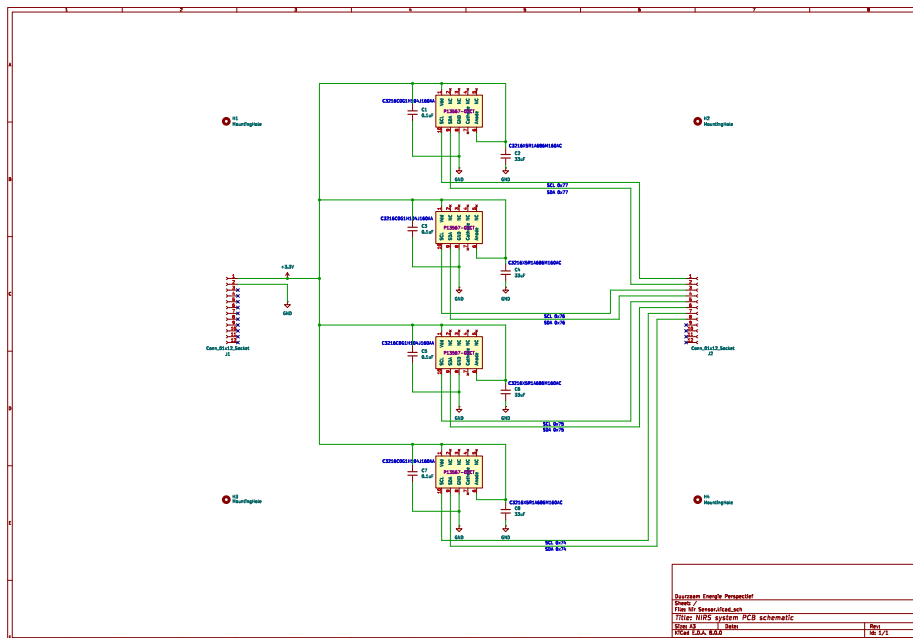


Figure B.1: Electrical schematic of the PCB.

# Appendix C

## Cable overview



Figure C.1: Overview of the used PLC cable with its cable tag and manufacturing year.